An invited review to the centenary of the National Academy of Sciences of Ukraine

https://doi.org/10.15407/ujpe63.11.1006

M.D. GLINCHUK,[1] V.V. KHIST [2]

[1] I.M. Frantsevych Institute for Problems of Materials Science, Nat. Acad. of Sci. of Ukraine
(3, Krzhyzhanivs'kyi Str., Kyiv 03142, Ukraine)

[2] Institute of Magnetism, Nat. Acad. of Sci of Ukraine and Ministry of Education and Science, Youth and Sport of Ukraine
(36, Academician Vernads'kyi Blvd., Kyiv 03680, Ukraine; e-mail: khist2012@gmail.com)

RENOVATION OF INTEREST IN THE MAGNETOELECTRIC EFFECT IN NANOFERROICS

Recent theoretical studies of the influence of the magnetoelectric effect on the physical properties of nanosized ferroics and multiferroics have been reviewed. Special attention is focused on the description of piezomagnetic, piezoelectric, and linear magnetoelectric effects near the ferroid surface in the framework of the Landau–Ginzburg–Devonshire phenomenological theory, where they are considered to be a result of the spontaneous surface-induced symmetry reduction. Therefore, nanosized particles and thin films can manifest pronounced piezomagnetic, piezoelectric, and magnetoelectric properties, which are absent for the corresponding bulk materials. In particular, the giant magnetoelectric effect induced in nanowires by the surface tension is possible. A considerable influence of size effects and external fields on the magnetoelectric coupling coefficients and the dielectric, magnetic, and magnetoelectric susceptibilities in nanoferroics is analyzed. Particular attention is paid to the influence of a misfit deformation on the magnetoelectric coupling in thin ferroic films and their phase diagrams, including the appearance of new phases absent in the bulk material. In the framework of the Landau–Ginzburg–Devonshire theory, the linear magnetoelectric and flexomagnetoelectric effects induced in nanoferroics by the flexomagnetic coupling are considered, and a significant influence of the flexomagnetic effect on the nanoferroic susceptibility is marked. The manifestations of size effects in the polarization and magnetoelectric properties of semiellipsoidal bismuth ferrite nanoparticles are discussed.

K e y w o r d s: ferroics, multiferroics, nanoferroics, Landau–Ginzburg–Devonshire theory, magnetoelectric effect.

1. Introduction

A considerable growth of the interest in materials demonstrating a correlation between ferromagnetic and ferroelectric properties has been observed in the last decade. Magnetoelectric (ME) materials [1, 2] with the coexisting ferromagnetic (FM) and ferroelectric (FE) orderings belong to multiferroics, which is schematically illustrated in Fig. 2.1. Till the beginning of the 21st century, magnetoelectrics and multiferroics were only interesting to a narrow circle of specialists, because ME effects could be observed only at low temperatures, so that there was no talking about the practical application of those effects. A recent burst in the research activity in this area is associated with the discovery of materials that have ME properties at room temperature and moderate magnetic fields.

2. Linear Magnetoelectric Effect

The physics of ME phenomena, which is actively developed, belongs to the fundamental problems dealing with the interrelation between the electric and magnetic fields. Similarly to electromagnetism, it is described by Maxwell's equations. However, despite their external resemblance, the ME phenomena are effects of different nature. Electromagnetic fields are intrinsically connected with electrodynamics; i.e. they arise only when electric charges move. At the same time, the ME effects are not reduced to dynamic phenomena. Even the static electric field generates a magnetization, and the static magnetic field generates an electric polarization.

First assumptions about the existence of substances whose molecules become magnetized by the electric field and electrified by the magnetic one were made as long ago as by Pierre Curie [4]. However, no ME materials, neither in the form of composites nor in the form of single-phase media, have been created till the middle of the 20th century.

In 1956, L.D. Landau and E.M. Lifshitz [5] made the notion of ME materials more accurate. Namely, those substances were classed to magnetoelectrics, whose symmetry allows the existence of linear ME effects, i.e. the emergence of the electrical polarization proportional to the magnetic field (direct ME effect), and the magnetization proportional to the electric field (inverse ME effect):

$$\mathbf{M} = \frac{\hat{\boldsymbol{\alpha}}}{4\pi}\mathbf{E}, \tag{2.1a}$$

$$\mathbf{P} = \frac{\hat{\boldsymbol{\alpha}}}{4\pi}\mathbf{H}, \tag{2.1b}$$

where $\mathbf{M}$ is the magnetization vector, $\mathbf{E}$ the electric field vector, $\mathbf{P}$ the polarization vector, $\mathbf{H}$ the magnetic field vector, and $\hat{\boldsymbol{\alpha}}$ the tensor of the linear ME effect. Note that formulas (2.1) couple vectors with different transformation properties with respect to the space (P) and time (T) inversion operations: the polar vectors $\mathbf{P}$ and $\mathbf{E}$ change their direction at the space inversion and remain invariable at the time inversion (i.e. they are P-odd and T-even vectors), whereas the axial vectors $\mathbf{M}$ and $\mathbf{H}$ are T-odd and P-even ones. Thus, a necessary condition for the existence of the linear ME effect in a substance is the separate violation of the P- and T-parity with the preservation of the combined PT-parity, which drastically narrowed the search scope for magnetoelectrics. In 1959, I.E. Dzyaloshinskii theoretically predicted the ME effect in Cr_2O_3 [6]. In a year, D.N. Astrov registered a magnetization induced by the electric field [see Eq. (2.1a)] [7]. Soon, V. Folen, G. Rado, and E. Stalder [8] changed the electric polarization induced in Cr_2O_3 by a magnetic field.

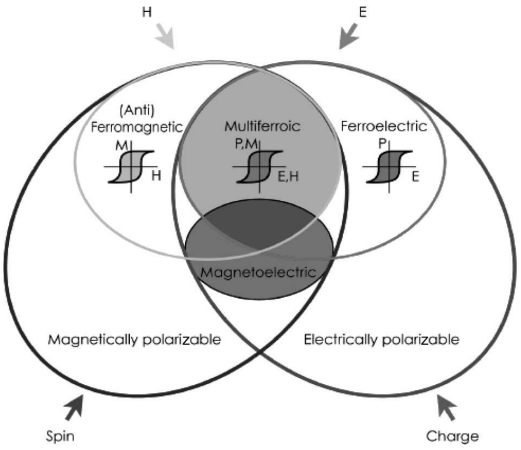

Fig. 2.1. Ferroics, multiferroics, and magnetoelectrics (reproduced from Ref. [3])

New materials with the ME effect as a cornerstone of new physical properties are the topic of this review. Their search is carried out very intensively, because ME materials open up broad prospects for their application in information and energy-saving technologies. They can serve as a basis for the creation of magnetic sensors, capacitance electromagnets, elements of magnetic memory, microwave filters, and other devices free of direct electric currents giving rise to heat losses. Some applications, e.g. sensors, are already at the practical implementation stage, the others are under development, whereas some things exist in the form of ideas.

Magnetic sensors are the most obvious and the most developed idea of the practical application of the ME effect. On the basis of composite ME materials, sensors of dc and ac fields are created with a sensitivity that far exceeds the sensitivity of sensors on the basis of the Hall effect and the giant magnetic resistance in the frequency interval 10^{-2}–10^{3} Hz [9]. At the same time, they are much cheaper than SQUIDs, which makes it possible to talk about the application of those magnetic sensors even in such domains as magnetoencephalography and magnetocardiography.

In this review, special attention is paid to nanostructured materials. These materials renew interest

in the ME effect in ferroics. Here, the existence of the surface plays a crucial role in the emergence of abnormal properties that are not observed in bulk materials.

2.1. Analysis of the symmetry of piezomagnetic, piezoelectric, and linear magnetoelectric effects induced by the surface

From the viewpoint of both fundamental and applied physics, the most interesting properties of nanomaterials are those, which are absent in bulk materials: antiferroelectric, ferroelectric, antiferromagnetic, and size-induced ferromagnetic ones. Since the translational symmetry is violated at any surface or interface, the structural modifications and the modifications in the polarization, magnetic, and electron states usually take place in thin films and nanoparticles [10, 11, 15–17].

The ME effect in nanomaterials has attracted a keen attention in the recent years [18]. The magnitude of the ME effect turned out much larger than that in the bulk. The evidence in favor of this assertion follows from the measurements of ME coefficients in bulk crystals and epitaxial $BiFeO_3$ films on the $SrTiO_3$ substrate. This effect is associated with the influence of boundary conditions [19]. Using the theory of symmetry, Eliseev *et al.* [20] determined how the surface-induced symmetry violation results in the appearance of spontaneous suface piezomagnetic, piezoelectric, and magnetoelectric effects in nanomaterials.

2.2. Surface piezomagnetic, piezoelectric, and linear magnetoelectric effects in nanosystems

For any spatially confined system, the inversion center disappears in the direction normally to the surface; only the symmetry axis and the planes normal to the surface survive. Hence, the magnetic and spatial symmetry group should be reduced to one of its subgroups consisting of the transformation matrices A_{ij}^S that satisfy the relation $n_i A_{ij}^S n_j = 1$, where n_j are the components of the unit vector normal to the surface.

The transformation law for the components of the linear ME-effect tensor γ_{ij}^S near the surface looks like

$$\tilde{\gamma}_{ij}^S = (-1)^{tr} \det\left(\mathbf{A}^S\right) A_{ik}^S A_{il}^S \gamma_{kl}^S,$$

with $\tilde{\gamma}_{ij}^S \equiv \gamma_{ij}^S$ for nonzero components. This law differs from the corresponding law for the bulk material,

$$\tilde{\gamma}_{ij} = (-1)^{tr} \det\left(\mathbf{A}\right) A_{ik} A_{il} \gamma_{kl},$$

by the form of transformation matrices $A_{ij}^S \neq A_{ij}$. The ME effect was demonstrated to exists in 58 magnetic classes of bulk materials [14]. Our analysis of the piezomagnetic tensor [20, 21] showed that the ME effect exists in nanosystems belonging to 90 magnetic classes.

The following formulas describing the size effect on the ME coupling in nanosystems were derived in work [20]:

- a thin film h in thickness on a rigid substrate,

$$\gamma_{3j}^R = \gamma_{3j} + \frac{\gamma_{3j}^S}{h} + \frac{d_{3kl}^{(\mathrm{Se})} d_{jkl}^{(\mathrm{Sm})}}{h^2\left(s_{11}+s_{12}\right)};$$

- a wire of radius R,

$$\gamma_{ij}^R = \gamma_{ij} + \frac{2}{R}\gamma_{ij}^S;$$

- a sphere of radius R,

$$\gamma_{ij}^R = \gamma_{ij} + \frac{3}{R}\gamma_{ij}^S.$$

2.3. Giant magnetoelectric effect induced in nanowires by the surface tension

Let us consider ferroics in the form of nanowires with two order parameters, the magnetization M and the electric polarization P. These order parameters can be either inherent to the bulk material or induced by the nanowire surface. Taking into account that ferromagnetism was observed at room temperature in nanoparticles 7–30 nm in diameter [10], whereas the ferroelectric state appears at a size of about 50 nm [11], nanowires of about 5–50 nm in size are usually studied. For such small dimensions, the influence of surfaces and boundary conditions associated with them, including the surface tension, is known to be strong. Therefore, the expected properties should be closer to those observed near the surface than to the bulk ones. Although with the growth of a specimen size, the properties gradually change from the surface (shell) to the bulk (core) ones (see, e.g., works [22, 23]), they can be considered uniform and subjected to a strong action of the surface tension, if the specimen size does not exceed 50 nm. The study of

ferroelectric nanoparticles with the use of the electron spin resonance (ESR) method showed [24] that the shell size varies from a few to tens of nanometers. A characteristic feature of the shell is the absence of spatial symmetry inversion. Therefore, the piezoelectric effect is possible even in the case of cubic symmetry in the bulk. In the general case, the existence of the piezomagnetic effect is not excluded.

Now, let us consider long cylindrical ferroic nanowires ($h \gg R$) electrically polarized along their axis z and magnetized along one of three equivalent axes. Let a nanowire with mechanically free side walls ($\rho = R$) be clamped between a plate ($z = -h/2$) and an upper electrode ($z = +h/2$) (see Fig. 2.2). The external electric and magnetic fields are applied along the axes z and x, respectively. In this geometry, there is no depolarization field. The demagnetization field can also be made low [5]. This geometry is typical of the majority of experiments. Under those conditions, a single-domain state is the most beneficial energetically. The electro- and magnetostriction effects, the mechanical strain tensor, and the boundary conditions at the curved nanoparticle surface have to be taken into account. The nanowires are assumed to be well separated from one another and do not interact electrically or magnetically.

The expansion of the Gibbs energy in a series of the uniform polarization P_3, magnetization M_1, and mechanical stress σ_{ij} looks like [13]

$$
\begin{aligned}
G_R = 2\pi h \int_0^R \rho\, d\rho \times \\
\times \Big(a_1 P_3^2 + a_{11} P_3^4 + a_{111} P_3^6 - \big(Q_{11}\sigma_{33} + \\
+ Q_{12}\left(\sigma_{11} + \sigma_{22}\right)\big) P_3^2 + \\
- \frac{1}{2}\left(A_{11}\sigma_{11}^2 + A_{11}\sigma_{22}^2 + A_{33}\sigma_{33}^2\right) P_3^2 + \ldots - \\
- g_{3jk}^e \sigma_{jk} P_3 + b_1 M_1^2 + b_{11} M_1^4 + a_{111} M_1^6 - \\
- \left(Z_{11}\sigma_{33} + Z_{12}\left(\sigma_{11} + \sigma_{22}\right)\right) M_1^2 - \\
- \frac{1}{2}\left(B_{11}\sigma_{11}^2 + B_{11}\sigma_{22}^2 + B_{33}\sigma_{33}^2\right) M_1^2 + \ldots - \\
- g_{1jk}^m \sigma_{jk} M_1 - \frac{1}{2} s_{11}\left(\sigma_{11}^2 + \sigma_{22}^2 + \sigma_{33}^2\right) - \\
- s_{12}\left(\sigma_{11}\sigma_{22} + \sigma_{11}\sigma_{33} + \sigma_{33}\sigma_{22}\right) - \\
- \frac{1}{2} s_{44}\left(\sigma_{23}^2 + \sigma_{13}^2 + \sigma_{12}^2\right) + \\
+ f_{ijkl}\sigma_{ij}^2\sigma_{kl}^2 - M_1 H_0 - P_3 E_0 \Big).
\end{aligned}
\tag{2.2}
$$

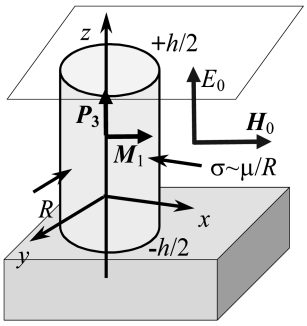

Fig. 2.2. A long cylindrical nanowire: x is one of three equivalent axes of weak magnetic anisotropy, and z is the axis od ferroelectric polarization. An external electric field is applied along the polarization axes, and the magnetic one along the x-axis (Reproduced from [[13]], with the permission of AIP Publishing)

Here, subscripts 1, 2, and 3 correspond to the Cartesian coordinates x, y, and z, respectively. Below, we will use the Voight or matrix notation, if necessary: $xx = 1$, $yy = 2$, $zz = 3$, $zy = 4$, $zx = 5$, and $xy = 6$. In the framework of the Landau–Ginzburg approach, the coefficients $a_1(T)$ and $b_1(T)$ depend linearly on the temperature T. All higher-order coefficients are assumed to be temperature-independent. We also assume that the order parameters and the spatial distribution of elastic stresses are uniform in a nanowire, so that the gradient energy can be neglected. Note that, in the case of the film-on-substrate geometry, this assumption is valid, if the film thickness does not exceed the critical thickness of the misfit deformation emergence, which is known to reach tens of nanometers [25].

The quantities Q_{ij} and Z_{ij} in Eq. (2.2) are the coefficients of the electro- and magnetostriction tensors, respectively; and s_{ij} are the components of the elastic compliance tensor [26]. Below, we assume that the symmetry of the piezoelectric, g_{3jk}^e, and piezomagnetic, g_{3jk}^m, tensors differs from the cubic one due to the surface effect: $g_{3jk}^e\sigma_{jk}P_3 = g_{31}^e(\sigma_{11}+\sigma_{22})P_3 + g_{33}^e\sigma_{33}P_3$, and $g_{1jk}^m\sigma_{jk}M_1 = g_{11}^m(\sigma_{11}+\sigma_{22})M_1 + g_{13}^m\sigma_{33}M_1$.

The distribution of stresses σ_{ij} must satisfy mechanical equilibrium conditions and boundary conditions at the curved nanoparticle surface,

$$
\begin{aligned}
&\frac{\partial \sigma_{ij}}{\partial x_i} = 0, \\
&\sigma_{\rho\rho}\big|_{\rho=R} = -\frac{\mu}{R}, \quad \sigma_{\rho\varphi}\big|_{\rho=R} = 0, \\
&\sigma_{\rho z}\big|_{\rho=R} = 0, \quad u_3(z = \pm h/2) = 0.
\end{aligned}
\tag{2.3}
$$

where $\mu_{ij} = \mu\delta_{ij}$ are coefficients of the surface stress tensor at the nanowire surface [27, 28]. The surface tension μ substantially depends on the nanowire material.

The minimization of the free energy with respect to the components σ_{ij} brings us to the equations $\partial G_R/\partial\sigma_{ij} = -u_{ij}$, where u_{ij} are components of the strain tensor. By neglecting the components $\sim f_{ijkl}\sigma_{ij}^2\sigma_{kl}^2$ and higher-order ones, we obtain the following homogeneous solution for the stresses tensor components σ_{ij} in the Cartesian coordinates [13]:

$$\sigma_{11} = \sigma_{22} = -\frac{\mu}{R}, \quad \sigma_{12} = \sigma_{13} = \sigma_{23} = 0, \tag{2.4}$$

$$\sigma_{33} = \frac{s_{12}(2\mu/R) - Q_{11}P_3^2 - Z_{11}M_1^2 - g_{33}^e P_3 - g_{13}^m M_1}{s_{11} + A_{33}P_3^2 + B_{33}M_3^2}. \tag{2.5}$$

As a rule, the shell thickness $\Delta h_d \approx 5 \div 50$ nm. In what follows, we consider a situation where $R < \Delta h_d$, i.e. all particles are in the shell, because it is the most important factor for the surface and size effects to manifest themselves.

We would like to emphasize that the considered mechanical boundary conditions are related to one of the possible experimental situations. The corresponding calculations showed that there is no ME coupling in mechanically free rods. At the same time, if a rod is partially clamped, the results obtained are qualitatively similar to those discussed below.

Furthermore, we assume that the quantities $A_{ii}\sigma_{ii}^2 P_3^2$ and $B_{ii}\sigma_{ii}^2 M_1^2$ are small, and we may neglect their higher powers. Substituting Eqs. (2.4), (2.5) into Eq. (2.2), we obtain the Gibbs energy with renormalized coefficients [13]:

$$G_R = 2\pi h \int_0^R \rho\, d\rho \Big(\alpha_1(T,R)P_3^2 + \alpha_{11}P_3^4 - \\ - P_3\left(E_0^+ E_p(R)\right) + \beta_1(T,R)M_1^2 + \\ + \beta_{11}M_1^4 + M_1\left(H_0^+ H_p(R)\right) + g_{\rm ME}(P_3, M_1)\Big). \tag{2.6}$$

The renormalized coefficients in front of P_3^2 and M_1^2 in the free energy (2.6) read

$$\alpha_1(T,R) = a_1(T) + \frac{\left(g_{33}^e\right)^2}{2s_{11}} + \\ + \frac{2\mu}{R}\left(Q_{12} - Q_{11}\frac{s_{12}}{s_{11}}\right) - \frac{2\mu^2}{R^2}\left(A_{11} + A_{33}\frac{s_{12}^2}{s_{11}^2}\right), \tag{2.7a}$$

$$\beta_1(T,R) = b_1(T) + \frac{\left(g_{13}^m\right)^2}{2s_{11}} + \\ + \frac{2\mu}{R}\left(Z_{12} - Z_{11}\frac{s_{12}}{s_{11}}\right) - \frac{2\mu^2}{R^2}\left(B_{11} + B_{33}\frac{s_{12}^2}{s_{11}^2}\right). \tag{2.7b}$$

The internal "built-in" fields induced by the piezoelectric and piezomagnetic effects look like

$$E_p(R) = \left(\frac{s_{12}}{s_{11}}g_{33}^e - g_{31}^e\right)\frac{4\mu}{R}, \\ H_p^(R) = \left(\frac{s_{12}}{s_{11}}g_{13}^m - g_{11}^m\right)\frac{4\mu}{R}. \tag{2.8}$$

The magnetoelectric energy density equals

$$g_{\rm ME} = (\gamma_{11}M_1P_3 + \gamma_{12}M_1P_3^2 + \gamma_{21}M_1^2P_3 + \gamma_{22}M_1^2P_3^2), \tag{2.9}$$

where the linear and quadratic coefficients of ME coupling look like

$$\gamma_{11} = \frac{g_{33}^e g_{13}^m}{s_{11}}, \tag{2.10a}$$

$$\gamma_{12} = g_{13}^m\left(\frac{Q_{11}}{s_{11}} + \frac{2\mu}{R}\frac{s_{12}A_{33}}{s_{11}^2}\right), \\ \gamma_{21} = g_{33}^e\left(\frac{Z_{11}}{s_{11}} + \frac{2\mu}{R}\frac{s_{12}B_{33}}{s_{11}^2}\right), \tag{2.10b}$$

$$\gamma_{22} = \left(\frac{Q_{11}Z_{11}}{s_{11}} - \frac{A_{33}\left(g_{13}^m\right)^2 + B_{33}\left(g_{33}^e\right)^2}{2s_{11}^2} + \right. \\ \left. + \frac{2\mu}{R}\frac{s_{12}}{s_{11}^2}\left(Q_{11}B_{33} + Z_{11}A_{33}\right) + \frac{4\mu^2}{R^2}\frac{s_{12}^2}{s_{11}^3}B_{33}A_{33}\right). \tag{2.10c}$$

For the coefficient of linear coupling to be nonzero, $\gamma_{11} \neq 0$, both the piezoelectric, g_{33}^e, and piezomagnetic, g_{13}^m, coefficients have to differ from zero, which is possible in a few special cases. For instance, $g_{33}^m = 1.2\times10^{-8}$ Wb/N and $g_{13}^m = -5.8\times10^{-9}$ Wb/N in the bulk of Terfenol-D [29].

2.4. Influence of size effects on the ME coupling coefficients

Let us rewrite Eqs. (2.10) in the form [13]:

$$\gamma_{12}(R) = \gamma_{12}^b\left(1 + \frac{R_{12}}{R}\right), \\ \gamma_{21}(R) = \gamma_{21}^b\left(1 + \frac{R_{21}}{R}\right), \\ \gamma_{22}(R) \approx \gamma_{22}^b\left(1 + \frac{R_{22}}{R}\right), \tag{2.11}$$

where

$$\gamma_{12}^b = g_{13}^m \frac{Q_{11}}{s_{11}}, \quad R_{12} = 2\mu \frac{s_{12}A_{33}}{s_{11}Q_{11}}, \quad \gamma_{21}^b = g_{33}^e \frac{Z_{11}}{s_{11}},$$
$$R_{21} = 2\mu \frac{s_{12}B_{33}}{s_{11}Z_{11}}, \quad \gamma_{22}^b = \frac{Q_{11}Z_{11}}{s_{11}} -$$
$$- \frac{A_{33}\left(g_{13}^m\right)^2 + B_{33}\left(g_{33}^e\right)^2}{2s_{11}^2}.$$

As a rule, the magnetoelectric constants in a bulk material are small or equal to zero, depending on the symmetry.

The coefficients of linear ME coupling do not depend on the nanoparticle radius, whereas the quadratic coefficients are reciprocal to this parameter. Thus, the latter coefficients strongly increase as the nanoparticle radius decreases. The linear ME coupling, γ_{11}, violates the symmetry $P \to -P$ and $M \to -M$ and also smears the transition point even in the zero magnetic and electric fields. Hence, Eqs. (2.11) mean the renormalization and do not exclude a possibility induced by the surface tension that $\gamma_{ij\neq 11}$ will change its sign, because the typical values of the parameters R_{ij} can be positive or negative. According to estimates [13], those values usually vary from 1 to 100 nm.

2.5. Calculation of susceptibilities

In terms of the renormalized coefficients, the free energy density $\tilde{g}(R,T)$ can be rewritten as follows:

$$\tilde{g}(R,T) = \Big(\alpha_1 P_3^2 + \beta_1 M_1^2 + \alpha_{11} P_3^4 + \beta_{11} M_1^4 -$$
$$- (E_p + E_0) P_3 - (H_p + H_0) M_1 + \gamma_{11} M_1 P_3 +$$
$$+ \gamma_{12} M_1 P_3^2 + \gamma_{21} M_1^2 P_3 + \gamma_{22} M_1^2 P_3^2\Big). \qquad (2.12)$$

The coefficients α_1 and β_1 depend on the temperature and nanoparticle radius according to Eqs. (2.7). They can be rewritten in the form

$$\alpha_1 = \alpha_T \left(T - T_{\rm CE}(R)\right). \quad \beta_1 = \beta_T \left(T - T_{\rm CM}(R)\right).$$

The R-dependences of the Curie temperature for the ferroelectric, $T_{\rm CE}(R)$, and ferromagnetic, $T_{\rm CM}(R)$, transitions can be found in works [13, 15].

The conditions for the free energy minimum,

$$\partial\tilde{g}/\partial P_3 = 0, \quad \partial\tilde{g}/\partial M_1 = 0,$$

give rise to the system of equations of state

$$\begin{cases} 2\alpha_1 P_3 + \gamma_{11} M_1 + 2\gamma_{12} M_1 P_3^+ \gamma_{21} M_1^2 + \\ + 2\gamma_{22} P_3 M_1^2 + 4\alpha_{11} P_3^3 = E_p + E_0, \\ 2\beta_1 M_1 + \gamma_{11} P_3 + \gamma_{12} P_3^2 + \\ + 2\gamma_{21} M_1 P_3 + 2\gamma_{22} P_3^2 M_1 + 4\beta_{11} M_1^3 = H_p + H_0, \end{cases} \qquad (2.13)$$

from which the order parameters can be determined. After elementary transformations of Eqs. (2.13), the susceptibilities can be written in the form [13]

$$\chi_{\rm E} = \frac{\partial P_3}{\partial E_0} = \frac{2\left(\beta_1 + \gamma_{21} P_3 + \gamma_{22} P_3^2 + 6\beta_{11} M_1^2\right)}{\Delta\left(M_1, P_3\right)}, \qquad (2.14a)$$

$$\chi_{\rm ME} = \frac{\partial P_3}{\partial H_0} = \frac{\partial M_1}{\partial E_0} =$$
$$= -\frac{\gamma_{11} + 2\gamma_{12} P_3 + 2\gamma_{21} M_1 + 4\gamma_{22} M_1 P_3}{\Delta\left(M_1, P_3\right)}, \qquad (2.14b)$$

$$\chi_{\rm M} = \frac{\partial M_1}{\partial H_0} = \frac{2\left(\alpha_1 + \gamma_{12} M_1 + \gamma_{22} M_1^2 + 6\alpha_{11} P_3^2\right)}{\Delta\left(M_1, P_3\right)}, \qquad (2.14c)$$

where

$$\Delta\left(M_1 P_3\right) = \Big(4\left(\alpha_1 + \gamma_{12} M_1 + \gamma_{22} M_1^2 + 6\alpha_{11} P_3^2\right) \times$$
$$\times \left(\beta_1 + \gamma_{21} P_3 + \gamma_{22} P_3^2 + 6\beta_{11} M_1^2\right) -$$
$$- \left(\gamma_{11} + 2\gamma_{12} P_3 + 2\gamma_{21} M_1 + 4\gamma_{22} M_1 P_3\right)^2\Big). \qquad (2.15)$$

Let us analyze the simplified equations (2.13) and (2.14), which determine the polarization, magnetization, and susceptibility. Taking into account that those parameters are standard for the ferroelectric (FE) and ferromagnetic (FM) phases, we will focus our attention on the multiferroic ferroelectric-ferromagnetic (FEFM) phase. In the considered case of non-zero quadratic ME effect, Eqs. (2.13) are simplified to the form

$$\begin{cases} 2\alpha_1 P_3 + 4\alpha_{11} P_3^3 + 2\gamma_{22} M_1^2 P_3 = 0, \\ 2\beta_1 M_1 + 4\beta_{11} M_1^3 + 2\gamma_{22} M_1 P_3^2 = 0. \end{cases} \qquad (2.16)$$

From whence, the following expressions are obtained for the order parameters in the FEM phase:

$$\begin{cases} P_{\rm FEM}^2 = \dfrac{-2\alpha_1\beta_{11} + \beta_1\gamma_{22}}{4\alpha_{11}\beta_{11} - \gamma_{22}^2}, \\ M_{\rm FEM}^2 = \dfrac{-2\alpha_{11}\beta_1 + \alpha_1\gamma_{22}}{4\alpha_{11}\beta_{11} - \gamma_{22}^2}. \end{cases} \qquad (2.17)$$

The positiveness of the susceptibilities

$$\chi_{\rm E} = \frac{\beta_{11}}{2\left(-2\alpha_1\beta_{11} + \beta_1\gamma_{22}\right)},$$
$$\chi_{\rm M} = \frac{\alpha_{11}}{2\left(-2\alpha_{11}\beta_1 + \alpha_1\gamma_{22}\right)},$$
$$\chi_{\rm ME} = -\frac{\gamma_{22}}{4\left(4\alpha_{11}\beta_{11} - \gamma_{22}^2\right) M_{\rm FEM}P_{\rm FEM}} =$$
$$= \frac{\gamma_{22}}{2\sqrt{\beta_{11}\alpha_{11}}}\sqrt{\chi_{\rm E}\chi_{\rm M}}$$

is a necessary condition for the FEFM phase to be stable.

Using expressions (2.17), we obtain

$$\Delta\left(M_{\rm FEM}, P_{\rm FEM}\right) =$$
$$= 16\left(4\alpha_{11}\beta_{11} - \gamma_{22}^2\right) P_{\rm FEM}^2 M_{\rm FEM}^2,$$

so that Eqs. (2.14) can be rewritten as follows:

$$\chi_{\rm E} = \frac{\beta_{11}}{2\left(-2\alpha_1\beta_{11} + \beta_1\gamma_{22}\right)}, \tag{2.18}$$
$$\chi_{\rm M} = \frac{\alpha_{11}}{2\left(-2\alpha_{11}\beta_1 + \alpha_1\gamma_{22}\right)}, \tag{2.19}$$
$$\chi_{\rm ME} = -\frac{\gamma_{22}}{4\left(4\alpha_{11}\beta_{11} - \gamma_{22}^2\right) M_{\rm FEM}P_{\rm FEM}} =$$
$$= \frac{\gamma_{22}}{2\sqrt{\beta_{11}\alpha_{11}}}\sqrt{\chi_{\rm E}\chi_{\rm M}}. \tag{2.20}$$

One can see that, at the points where $P_{\rm FEM}^2$ or $M_{\rm FEM}^2$ equals zero, the susceptibility $\chi_{\rm ME}$ diverges. It should be emphasized that formula (2.18)–(2.20) for $\chi_{\rm ME}$ coincides with that obtained in work [11], $\gamma_{22} < 2\sqrt{\beta_{11}\alpha_{11}}$, which follows from the FEFM phase stability.

The coefficients α_1 and β_1 depend on the temperature and nanoparticle radius; namely,

$$\alpha_1 = \alpha_T\left[T - T_{\rm CE}(R)\right], \quad \beta_1 = \beta_T\left[T - T_{\rm CM}(R)\right].$$

Substituting these dependences into Eqs. (2.18), we obtain

$$\chi_{\rm E} = \frac{C_{\rm E}}{\left(T_{\rm CE}^* - T\right)}, \tag{2.21}$$
$$\chi_{\rm M} = \frac{C_{\rm M}}{\left(T_{\rm CM}^* - T\right)}, \tag{2.22}$$
$$\chi_{\rm ME} = \frac{\gamma_{22}}{2\sqrt{\alpha_{11}\beta_{11}}}\sqrt{\frac{C_{\rm E}C_{\rm M}}{\left(T_{\rm CT}^* - T\right)\left(T_{\rm CM}^* - T\right)}}. \tag{2.23}$$

In expressions (2.21)–(2.23), we introduced the Curie–Weiss temperatures and constants renormalized due to the ME coupling,

$$T_{\rm CE}^* = \frac{2\beta_{11}\alpha_T T_{\rm cl}(R) - \beta_T\gamma_{22}T_{\rm CM}(R)}{2\beta_{11}\alpha_T - \beta_T\gamma_{22}}, \tag{2.24a}$$
$$T_{\rm CM}^* = \frac{2\alpha_{11}\beta_T T_{\rm CM}(R) - \alpha_T\gamma_{22}T_{\rm cl}(R)}{2\alpha_{11}\beta_T - \alpha_T\gamma_{22}}, \tag{2.24b}$$
$$C_{\rm E} = \frac{\beta_{11}}{2(2\alpha_T\beta_{11} - \beta_T\gamma_{22})}, \tag{2.24c}$$
$$C_{\rm M} = \frac{\alpha_{11}}{2(2\alpha_{11}\beta_T - \alpha_T\gamma_{22})}. \tag{2.24d}$$

Equations (2.17) can be rewritten in the form

$$P_{\rm FEM}^2 = A_{\rm E}(T_{\rm CE}^* - T), \tag{2.25a}$$
$$M_{\rm FEM}^2 = A_{\rm M}(T_{\rm CM}^* - T), \tag{2.25b}$$

where the constants

$$A_{\rm E} = \frac{2\alpha_T\beta_{11} - \beta_T\gamma_{22}}{4\alpha_{11}\beta_{11} - \gamma_{22}^2}, \quad A_{\rm M} = \frac{2\alpha_{11}\beta_T - \alpha_T\gamma_{22}}{4\alpha_{11}\beta_{11} - \gamma_{22}^2} \tag{2.26}$$

were introduced. Therefore, we obtain a standard formula for the order parameters and susceptibilities, but with the magnetoelectric coupling, transition temperature, and other coefficients renormalized by the size effect. Note that the variants of the EE and FM phases can be obtained from Eqs. (2.23)–(2.26) by putting $\gamma_{22} \to 0$.

2.6. Influence of external fields on the polarization and susceptibility

The polarization P_3 is a ferroelectric order parameter. In Fig. 3.1, *a*, this is shown for the zero electric field ($E = 0$) and a few magnetic fields H_0 (normalized to the coercive field) for the positive coefficient $\Gamma_{22}(R) > 0$ and two values of the nanowire radius $R/R_Q = 10$ (curves *1*) and 3 (curves *2*). The temperature dependences of the susceptibilities $\chi_{\rm E}$ and $\chi_{\rm ME}$ are exhibited in Fig. 3.1, *b* and 3.1, *c*, respectively. Figure 3.1, *d* demonstrates the temperature dependence of the dielectric susceptibility $\delta\chi_{\rm E} = (\chi_{\rm E}(H) - \chi_{\rm E}(0))/\chi_{\rm E}(0)$.

From Fig. 3.1, *a*, one can see that, as the magnetic field grows, the ferroelectric order parameter decreases, and the phase transition at low temperatures (cusps in the solid curves) is smeared. If

the magnetic field induced by the ME coupling is sufficiently large, it can suppress the ferroelectric polarization, which occurs under the condition $\alpha_1 + \gamma_{22} M_1^2 \geq 0$, i.e. when the binding energy $\gamma_{22} M_1^2 P_3^2$ suppresses the FE phase, as is shown by curves *2*. Additional calculations testify that the transition into the FEFM phase takes place at a negative γ_{22}-value. At the same time, the transition temperature between the ferroelectric and paraelectric phases changes weakly.

Figure 3.1, *b* demonstrates that the dielectric susceptibility $\chi_{\rm E}$ increases with H_0, as one should expect in the case of decreasing polarization.

As follows from Fig. 3.1, *c*, the magnetoelectric susceptibility has a singularity at the transition point between the FEFM and FE phases in the zero magnetic field (the solid curves).

Finally, Fig. 3.1, *d* illustrates that the dielectric susceptibility increases, as the magnetic field grows. Its gigantic value at small nanoparticle radii is associated with the FEFM-FM transition; the latter is induced by the ME coupling and takes place at positive γ_{22} -values. Narrow peaks (singularities) of the susceptibility at high temperatures emerge due to the weak dependence of the high-temperature susceptibility peaks on the magnetic field (see Fig. 3.1, *b*). The dielectric susceptibility grows enormously (by a factor of 10 and more) near the phase transitions (cf. the 500%-effect shown in work [16]). Those effects are not observed in the bulk material, which allows the small coefficients of ME coupling in the bulk to be neglected.

3. Influence of a Misfit Deformation on the Magnetoelectric Coupling in Thin Ferroic Films

As was reported in works [30, 31], thin deformed hetero-epitaxial $BiFeO_3$ films demonstrate the much higher ME coefficients and spontaneous polarization in comparison with the bulk material. Similar effects were also observed in thin polycrystalline films [19, 32].

In this section, we demonstrate that the misfit deformation, which arises owing to the mismatch of crystal lattices at the film-substrate interface, can strongly change the ME coupling coefficients, the surface energy parameters, and the polar and magnetic phase diagrams of antiferromagnetic ferroelectric films. This effect makes it possible to extend the interval of the electrical and magnetic properties of the films, which opens ways to their new applications.

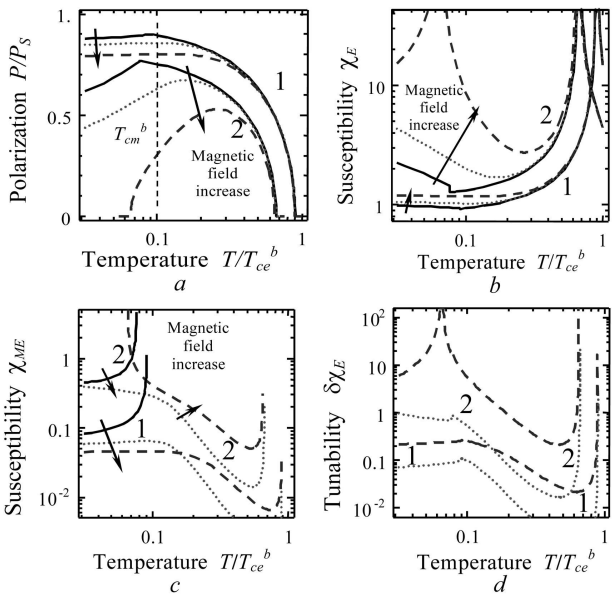

Fig. 3.1. Temperature dependences of the polarization P_3 (*a*), dielectric susceptibility $\chi_{\rm E}$ (*b*), magnetoelectric susceptibility $\chi_{\rm ME}$ (*c*), and dielectric tunability $\delta\chi_{\rm E}$ (*d*) in the zero electric field and various magnetic fields $H_0/H_{\rm C} = 0$ (solid curves), 0.3 (dotted curves), and 1 (dashed curves) for nanowires with a large ($R/R_Q = 10$, curves *1*) and a small ($R/R_Q = 3$, curves *2*) radius (Reproduced from [13], with the permission of AIP Publishing)

3.1. Free energy functional

Let us consider an antiferromagnetic ferroelectric film that was epitaxially grown on a thick rigid substrate. The film has the thickness l and occupies the space region $-l/2 \leq z \leq l/2$. It is in a perfect electrical contact with thin electrodes. For simplicity, we assume that the piezomagnetic effect is absent, whereas magnetostriction does exist inside the film.

In accordance with the phenomenological Landau–Ginzburg–Devonshire theory, the Gibbs free energy looks like

$$\Delta G = \frac{1}{l} \int\limits_{-l/2}^{l/2} dz g_V(z) + G_S\left(\frac{l}{2}\right) + G_S\left(-\frac{l}{2}\right), \quad (3.1)$$

where g_V and G_S are the bulk and surface, respectively, densities of the film free energy. When describing the phase transitions in antiferromagnetic ferro-

electric films, we assume that their substance has two magnetic sublattices with the magnetization vectors $\mathbf{M}_a$ and $\mathbf{M}_b$. The polarization P_3 and the electric field E_0 are directed along the polar axis z. The axis x is considered to be the axis of weak magnetic anisotropy. When analyzing the size effects on the phase transitions in thin films, the dependence of the polarization P_3 and the magnetizations $\mathbf{M}_{a,b}$ of two sublattices on the depth z should be taken into consideration [14, 25]. The expansion of the Gibbs energy density g_V in a power series of the quantities P_3 and $\mathbf{M}_{a,b}$ looks like [33]:

$$g_V = \left(a_1 P_3^2 + a_{11} P_3^4 + a_{111} P_3^6 + \gamma \left(\frac{dP_3}{dz} \right)^2 - \right.$$
$$- Q_{ij33}\sigma_{ij} P_3^2 - \frac{A_{ij}}{2}\sigma_{ij}^2 P_3^2 - P_3 \left(E_0 + \frac{E_d}{2} \right) - \frac{s_{ijkl}}{2}\sigma_{ij}\sigma_{kl} \times$$
$$\times b \left(\mathbf{M}_a^2 + \mathbf{M}_b^2 \right) + c\mathbf{M}_a\mathbf{M}_b + d \left(\mathbf{M}_a^4 + \mathbf{M}_b^4 \right) +$$
$$+ k\,\mathbf{M}_a^2\mathbf{M}_b^2 + \delta \left(\frac{d\mathbf{M}_a}{dz} \right)^2 + \delta \left(\frac{d\mathbf{M}_b}{dz} - \right)^2 -$$
$$- \left(M_{a1} + M_{b1} \right) H_0 + b_1 \left(M_{a1}^2 + M_{b1}^2 \right) + c_1 M_{a1} M_{b1} -$$
$$\left. - Z_{ij11}\sigma_{ij} \left(M_{a1}^2 + M_{b1}^2 \right) - W_{ij11}\sigma_{ij} M_{a1} M_{b1} \right). \quad (3.2)$$

Subscripts 1, 2, and 3 correspond to the Cartesian coordinates x, y, and z, respectively. We assume that the bulk material has a cubic symmetry in the paraphase. Equation (3.2) makes allowance for the polarization, magnetic, and correlation energies, the interaction with the external field E_0, the electro- and magnetostriction energies, the elastic energy, and the energy of depolarization field E_d. The coefficients $a_1(T) = \alpha_{\mathrm{P}} \left(T - T_{\mathrm{C}}^b \right)$ and $b(T) = \alpha_{\mathrm{M}} \left(T - T_{\mathrm{N}}^b \right)$ are explicit functions of the temperature T, whereas all other coefficients in the expansion are assumed to be temperature-independent. The parameters T_{C}^b and T_{N}^b are the Curie and Neél transition temperatures, respectively; σ_{ij} are components of the elastic stress tensor; Q_{ijkl}, Z_{ijkl}, and W_{ijkl} are components of the electro- and magnetostriction tensors, respectively; and s_{ijkl} are components of the elastic strain tensor. Note that the demagnetization field is absent, if $(\mathbf{M}_{a,b})_3 = 0$. As a rule, $|b| \gg |c| \gg |b_1| + |c_1|$. For the antiferromagnetic (AFM) phase to be stable in the bulk specimen, the inequalities $2b_1 - c_1 < 0$ and $2b_1 - c_1 > 0$ must be satisfied.

In the case of a single-domain insulated film with perfect electrodes, the depolarization field $E_d = 4\pi \left[\bar{P}_3 - P_3(z) \right]$, where the bar means the average value over the film thickness, $\bar{P}_3 \equiv \frac{1}{l} \int_{-l/2}^{l/2} P_3(z)\, dz$.

The equilibrium equation can be obtained by varying the Gibbs energy with respect to the stress σ_{ij}, i.e. $\partial G_V / \partial \sigma_{jk} = -u_{jk}$. The misfit deformation $u_{11} = u_{22} = u_m \neq 0$ takes place at the film-substrate interface $z = -l/2$. The top surface of the film is free, so that the normal components $\sigma_{3j} = 0$ at $z = l/2$. The non-zero uniform stresses equal

$$\sigma_{11} = \frac{u_m}{s_{1111} + s_{1122} + A_{11} P_3^2} +$$
$$+ \frac{u_{22}^S s_{1122} - u_{11}^S \left(s_{1111} + A_{11} P_3^2 \right)}{\left(s_{1111} + A_{11} P_3^2 \right)^2 - s_{1122}^2}$$

and

$$\sigma_{22} = \frac{u_m}{s_{1111} + s_{1122} + A_{11} P_3^2} +$$
$$+ \frac{u_{11}^S s_{1122} - u_{22}^S \left(s_{1111} + A_{11} P_3^2 \right)}{\left(s_{1111} + A_{11} P_3^2 \right)^2 - s_{1122}^2},$$

where the spontaneous bulk deformations

$$u_{11}^S = Q_{1122} P_3^2 + Z_{1111} \left(M_{a1}^2 + M_{b1}^2 \right) + W_{1111} M_{a1} M_{b1},$$
$$u_{22}^S = Q_{1122} P_3^2 + Z_{1122} \left(M_{a1}^2 + M_{b1}^2 \right) + W_{1122} M_{a1} M_{b1}$$

were introduced. This homogeneous solution of the elastic problem is valid, if the film thickness does not exceed the critical thickness l_d of the dislocation appearance, which is known to amount to tens of nanometers. The effective misfit strain $u_m^*(l) = u_m l_d / l$ [34].

The inversion center disappears near the surface, and the near-surface piezoelectric effect g_{ijk}^e has to be taken into account in the surface free energy [15],

$$G_S \left(\pm \frac{l}{2} \right) = \frac{1}{l} \left(\frac{\delta}{\lambda_{\mathrm{M}}} \left(\mathbf{M}_a^2 + \mathbf{M}_b^2 \right) + \right.$$
$$\left. + \frac{\delta}{\lambda_{\mathrm{MA}}} \left(M_{a1}^2 + M_{b1}^2 \right) + \frac{\gamma}{\lambda_{\mathrm{P}}} P_3^2 - g_{3jk}^e \sigma_{jk} P_3 \right) \Big|_{z = \pm \frac{l}{2}}, \quad (3.3)$$

where λ_p, λ_{M}, and λ_{MA} are ferroelectric and magnetic, respectively, extrapolation lengths [34], with $\lambda_{\mathrm{MA}} \gg \lambda_{\mathrm{M}}$, which corresponds to the weak magnetic anisotropy conditions.

3.2. Influence of a misfit deformation on phase diagrams

Let us introduce the ferromagnetic, $\mathbf{M}_F = \mathbf{M}_a + \mathbf{M}_b$, and antiferromagnetic, $\mathbf{M}_A = \mathbf{M}_a - \mathbf{M}_b$, order parameters for two equivalent magnetic sublattices ($\mathbf{M}_a^2 = \mathbf{M}_b^2 = M^2$) [35]. Substituting the stress σ_{ij} into the Gibbs energy (3.1), performing the Legendre transformation, and using the direct variational method for the solution of the Euler–Lagrange equations, which was proposed in work [36], we obtain the Helmholtz free energy for various phases [33]:

$$F^{\mathrm{DP}}\left[\bar{P}_3, \bar{M}, \theta\right] \approx \Big(\alpha_{\mathrm{P}}\left(T - T_{\mathrm{cr}}^{FE}(l)\right)\bar{P}_3^2 + a_{11}^m \bar{P}_3^4 - \\ - (E_m + E_0)\,\bar{P}_3 + 16\tilde{d}\cdot\bar{M}^4 + 2\alpha_{\mathrm{M}}\left(T - T_{\mathrm{cr}}^{\mathrm{DP}}(l)\right)\bar{M}^2 + \\ + 4\tilde{f}^{\mathrm{DP}}(l)\bar{P}_3^2\bar{M}^2 + \Delta F^{\mathrm{DP}}\left[\bar{M}, \theta\right]\Big), \tag{3.4a}$$

$$\Delta F^{\mathrm{AFM}} = 0, \\ \Delta F^{\mathrm{FM}} = -2H_0\bar{M}, \tag{3.4b} \\ \Delta F^{\mathrm{FI}} \approx (2c + 4\tilde{c}_1)\,\bar{M}^2\overline{\cos\theta}^2 - 2H_0\overline{M}\,\overline{\cos\theta}.$$

Here, the superscript DP denotes the AFM, FM, or mixed ferrimagnetic (FI) phase, respectively.

Expressions for renormalized coefficients in Eqs. (3.4) are quoted in work [33]. In the AFM phase, the non-zero magnetization component is $M_{A1}(z) \equiv 2M(z)$, whereas the component $M_{F1}(z) \equiv \equiv 2M(z)$ vanishes in the FM phase. The dependence of the order parameters on the depth z is taken into account for the FI phase. In particular [5, 33], for the case of one domain and large extrapolation length λ_{MA},

$$\mathbf{M}_F(z) = (2M(z)\cos\theta(z), 0, 0), \\ \mathbf{M}_A(z) = (0, 2M(z)\sin\theta(z), 0), \\ \overline{\cos\theta} \approx \frac{H_0}{2\bar{M}\left(c + 2\tilde{c}_1 + 2\tilde{f}^{\mathrm{FM}}\bar{P}_3^2\right)}.$$

Provided the zero magnetic field, $H_0 = 0$, and the angle $\theta = \pi/2$, the absolute stability conditions are satisfied in the FI phase at the axes and the planes of weak magnetic anisotropy.

The averaged magnetization $\bar{M}$ depends on the polarization $\bar{P}_3$ through the ME coupling $\tilde{f}^{\mathrm{DP}}$,

$$\bar{M}^2 = -\Big(\alpha_{\mathrm{M}}\left(T - T_{\mathrm{cr}}^{\mathrm{DF}}(l)\right) + 2\tilde{f}^{\mathrm{DP}}\bar{P}_3^2\Big)/16\tilde{d}. \tag{3.5}$$

Therefore, the phase transitions induced by the ME coupling can take place. In the zero total field, $E_m + E_0 = 0$, each of phases (3.4) can be either paraelectric (PE) at $P_3 = 0$ or ferroelectric (FE) at $P_3 \neq 0$. The evaluation of material parameters shows that the size effects and misfit deformations significantly renormalize the free energy coefficients. Misfit deformations can considerably increase the values of the quadratic ME coupling coefficients $\tilde{f}^{\mathrm{AFM,FM}}(l)$ in comparison with the bulk values $f_{\pm}$.

It should be emphasized that the misfit deformation u_m and the film thickness l can change the order parameters $\bar{M} = \bar{M}(T, l, u_m)$ and $\bar{P}_3 = \bar{P}_3(T, l, u_m)$. As a result, the phase transitions associated with the size effects and ME coupling can take place. For more details, see work [33].

4. Linear Magnetoelectric Coupling Induced by the Flexomagnetic Effect in Nanoferroics

4.1. Brief review of the state-of-art

Non-uniform deformations and electric fields that can be induced by external forces or can spontaneously arise in systems with a non-uniform polarization distribution (e.g., the polarization change in a vicinity of the surface) bring about the flexoelectric coupling. The flexoelectric effect is a typical example, which is a result of the coupling between the polarization and the elastic deformation gradient (direct effect) and between the polarization gradient and the elastic deformation (inverse effect). The flexoelectric effect was theoretically studied in detail by Tagantsev [37]. The components of the flexoelectric tensor were experimentally measured in bulk perovskite crystals by Ma and Cross [38–42] and Zubko *et al.* [43]. The interest in the theoretical description of flexoelectric phenomena in various nanostructures was renewed by Catalan *et al.* [44, 45], Sharma *et al.* [46–48], and Kalinin and Meunier [49]. The spontaneous manifestation of the flexoelectric effect in ferroelectric nanoparticles owing to the internal gradients of the order parameter was considered by Eliseev *et al.* [50].

The flexomagnetic coupling is much less studied than the flexoelectric one. Only a few relevant articles have been published [51, 52]. In particular, proceeding from the first principles, Lukashev and Sabirianov managed to calculate a value of $1.95\mu_{\mathrm{B}}$ Å for the flexomagnetic coefficient of antiperovskite Mn_3GaN as

the coupling parameter between the electric voltage gradient and the magnetic dipole moment of the Mn atom.

It is worth emphasizing that the validity of only the time and/or spatial inversion operation is not enough for the flexomagnetic effect to exist. For the latter to take place, those operations must be related to each other in the material symmetry group. The study of a symmetry taking the flexomagnetic effect into account was carried out in the framework of the symmetry group theory, as was earlier done for the piezomagnetic [20, 21, 53] and ME [54–56] effects.

In this section, a new mechanism governing the appearance of the linear ME effect in multiferroics and (induced) ferroelectrics-(anti)ferromagnets is proposed It is associated with the existence of the flexomagnetic effect. Ferro-(anti)ferromagnetic multiferroics are extremely rare in the nature, especially as bulk materials. The proposed mechanism, besides the fundamental interest, may give rise to new technologies and, therefore, may be very important for various applications.

4.2. Linear flexomagnetic coupling in ferroelectric-ferromagnetic nanosystems

While describing the flexomagnetic coupling in spatially confined ferroelectric-ferromagnetic systems, the phenomenological Landau–Ginzburg–Devonshire approach is used [57–63]. In the framework of this approach, we can calculate the surface and gradient energies, the depolarization and demagnetization fields, the mechanical pressure, the flexoelectric and flexomagnetic effects. The bulk and surface contributions to the total free energy look like [64]:

$$F_V = \int\limits_V \big(g_{\rm FE} + g_{\rm FM} + g_{\rm elast} + \\ + g_{\rm striction} + g_{\rm flexo} + g_{\rm ME}\big) d^3r, \tag{4.1}$$

$$F_S = \int\limits_S d^2r \left(\frac{a_i^S}{2} P_i^2 + K_S \left(\mathbf{Mn}\right)^2\right), \tag{4.2}$$

where $\mathbf{P}$ is the polarization vector, $\mathbf{M}$ the magnetization vector, and $\mathbf{n}$ a normal to the surface. The constant K_S in the surface energy is responsible for the surface magnetic anisotropy (see work [63]). The coefficient a_i^S is considered to be positive. The dependence of the Gibbs energy density on the order parameters P and M are shown below.

The ferroelectric component of the free energy is equal to

$$g_{\rm FE} = \frac{a_{ij}^{(e)}(T)}{2} P_i P_j + \frac{a_{ijkl}^{(e)}}{4} P_i P_j P_k P_l + ... + \\ + \frac{g_{ijkl}^{(e)}}{2} \frac{\partial P_i}{\partial x_j} \frac{\partial P_k}{\partial x_l} - P_i E_i, \tag{4.3}$$

where E_i is the electric field component, and the tensor $g_{ijkl}^{(e)}$ determines the energy contribution of the polarization gradient and is assumed to be positive. The ferromagnetic component is equal to

$$g_{\rm FM} = \left(\frac{a_{ij}^{(m)}(T)}{2} M_i M_j + K \left(\mathbf{Mb}\right)^2 + \\ + \frac{g_{ijkl}^{(m)}}{2} \frac{\partial M_i}{\partial x_j} \frac{\partial M_k}{\partial x_l} - \mathbf{HM}\right), \tag{4.4}$$

where K is the uniaxial anisotropy constant, $\mathbf{b}$ a unit vector directed along the magnetic anisotropy axis, $\mathbf{H}$ the magnetic field vector, and the tensor $g_{ijkl}^{(m)}$, which is sometimes referred to as the "heterogeneous exchange interaction", determines the contribution of the magnetization gradient to the free energy. The elastic component to the free energy equals

$$g_{elast} = \frac{c_{ijkl}}{2} u_{ij} u_{kl}, \tag{4.5}$$

where u_{ij} is the strain tensor, and c_{ijkl} the elastic modulus tensor. The piezoelectric, piezomagnetic, electro-, and magnetostriction components are

$$g_{\rm striction} = -d_{ijk}^{(e)} P_i u_{jk} - d_{ijk}^{(m)} M_i u_{jk} - \\ - q_{ijkl}^{(e)} u_{ij} P_k P_l - q_{ijkl}^{(m)} u_{ij} M_k M_l, \tag{4.6}$$

where $d_{ijk}^{(e)}$ and $d_{ijk}^{(m)}$ are components of the tensors of the piezoelectric and piezomagnetic effects, respectively; and $q_{ijkl}^{(e)}$ and $q_{ijkl}^{(m)}$ are components of the tensors of the bulk electro- and magnetostriction effects, respectively.

The contribution of the flexomagnetic and flexoelectric couplings to the energy equals

$$g_{\rm flexo} = \frac{Q_{ijkl}^{(m)}}{2} \left(\frac{\partial u_{ij}}{\partial x_k} M_l - u_{ij} \frac{\partial M_l}{\partial x_k}\right) + \\ + \frac{Q_{ijkl}^{(e)}}{2} \left(\frac{\partial u_{ij}}{\partial x_k} P_l - u_{ij} \frac{\partial P_l}{\partial x_k}\right), \tag{4.7}$$

where $Q^{(m)}_{ijkl}$ and $Q^{(e)}_{ijkl}$ are the tensors of flexomagnetic and flexoelectric couplings, respectively. Note that the flexoelectric effect is not observed in the paramagnetic phase, although it exists for all types of symmetry.

The contribution of the magnetoelectric coupling to the free energy looks like

$$g_{\rm ME} = f_{ij} M_i P_j + w_{ijk} M_i P_j P_k + \dots . \tag{4.8}$$

This expression includes the bilinear term $f_{ij} M_i P_j$, which is relevant for 58 bulk magnetic classes and almost all surface magnetic classes inherent to nanosystems. The quadratic terms proportional to $M_i M_j P_k$ and $M_i M_j P_k P_l$ are usually small in comparison with the bilinear term.

In order to study the influence of flexolectricity and flexomagnetism on magnetoelectricity, we neglect the depolarization and demagnetization fields. For instance, we consider prolate particles, in which the magnetization and polarization are directed along the same axis.

Let us demonstrate the influence of a deformation and consider the case of a mechanically free system; i.e. the boundary conditions are $\sigma_{ij} n_i|_S = 0$. We assume that the field of mechanical stresses in nanosystems with a characteristic size of 10 nm is similar to the surface one, i.e. it can be taken to equal zero everywhere. Therefore, the surface tension can be easily determined explicitly. Substituting the solutions for the strain tensor into the free energy (4.1) and using the Legendre transformation, we obtain new terms in the ME and FMFE energies [64],

$$g_{\rm ME} = \left(f_{ij} + s_{wvqs} d^{(e)}_{jwv} d^{(m)}_{isq} \right) M_i P_j + \\ + \left(w_{ijk} + s_{wvqs} d^{(m)}_{iwv} q^{(e)}_{sqjk} \right) M_i P_j P_k, \tag{4.9a}$$

$$g_{\rm FME} = s_{ijqs} Q^{(m)}_{ijkl} Q^{(e)}_{qsnp} \frac{\partial M_k}{\partial x_l} \frac{\partial P_n}{\partial x_p} + \\ + s_{ijqs} Q^{(m)}_{ijkl} d^{(e)}_{nsq} P_n \frac{\partial M_l}{\partial x_k} + s_{ijqs} Q^{(e)}_{ijkl} d^{(m)}_{nsq} M_n \frac{\partial P_l}{\partial x_k} + \\ + s_{ijqs} Q^{(m)}_{ijkl} q^{(e)}_{qsnp} P_n P_p \frac{\partial M_k}{\partial x_l} + \\ + s_{ijqs} Q^{(m)}_{ijkl} q^{(e)}_{qsnp} P_n \frac{\partial P_p}{\partial x_l} M_k + \\ + s_{ijqs} q^{(m)}_{ijkl} Q^{(e)}_{qsnp} \frac{\partial P_n}{\partial x_p} M_k M_l + \\ + s_{ijqs} Q^{(e)}_{ijkl} q^{(m)}_{qsnp} P_n M_k \frac{\partial M_l}{\partial x_p}. \tag{4.9b}$$

Attention should be paid to that the flexomagnetic term in Eq. (4.9b) is absent from the expression for the initial free energy (4.1). The most important term is the linear flexomagnetoelectric term

$$g^S_{\rm FME} = s_{ijqs} Q^{(m)}_{ijkl} Q^{(e)}_{qsnp} \frac{\partial M_k}{\partial x_l} \frac{\partial P_n}{\partial x_p} + \\ + s_{ijqs} Q^{(m)}_{ijkl} d^{(e)}_{nsq} P_n \frac{\partial M_l}{\partial x_k} + s_{ijqs} Q^{(e)}_{ijkl} d^{(m)}_{nsq} M_n \frac{\partial P_l}{\partial x_k},$$

which exists in the absence of external factors – in particular, magnetic, electric, and elastic fields – due to the existence of the spontaneous magnetization and polarization gradients. The linear flexomagnetoelectric coupling is not associated with the piezoelectric effect and equals [64]

$$Q^{\rm FME}_{klnp} \equiv s_{ijqs} Q^{(m)}_{ijkl} Q^{(e)}_{qsnp}. \tag{4.10}$$

It is proportional to the product of the flexolectric, $Q^{(e)}_{ijkl}$, and flexomagnetic, $Q^{(m)}_{ijkl}$, tensors, whose values can be determined experimentally [39–42, 44] or calculated from the first principles [52]. The term $g^S_{\rm FME}$, as well as the terms $\sim Q^{(m)}_{ijkl} P_n P_p \frac{\partial M_k}{\partial x_l}$ and $\sim Q^{(m)}_{ijkl} P_n \frac{\partial P_p}{\partial x_l} M_k$ that are linear in the magnetization, are relevant for materials with the nonzero flexomagnetic tensor $Q^{(m)}_{ijkl}$. Those terms are responsible for the appearance of the non-uniform polarization and magnetization in spatially inhomogeneous ferromagnets. The terms proportional to the magnetization and its gradient, $\sim P_n M_k \frac{\partial M_l}{\partial x_p}$ and $\sim \frac{\partial P_n}{\partial x_p} M_k M_l$, are relevant for materials with an arbitrary symmetry, because the flexoelectric tensor $Q^{(e)}_{ijkl}$ and the magnetostriction tensor $q^{(m)}_{ijnp}$ have non-zero components in any case.

In Table 4.1, the symmetry groups of ferroelectrics-ferromagnets with the non-zero flexomagnetic effect ($Q^{(m)}_{ijkl} \neq 0$) are counted. It should be noted that all 13 ferromagnetic-ferroelectric groups in the table can be surface groups. All groups of ferroelectric-ferromagnets quoted in Table 4.1 are linear flexomagnetoelectrics, magnetoelectrics, piezomagnets, and piezoelectrics ($d^{(e)}_{ijk} \neq 0$ and $d^{(m)}_{ijk} \neq 0$) both in the bulk and near the surface. It should be emphasized that the number of non-zero tensor components is always several times larger than the number of non-trivial components.

Table 4.1. **Ferromagnets-ferroelectrics with the flexomagnetic effect (multiferroics of type I [64])**

Point symmetry group	Magnetic symmetry group	Number of non-trivial (non-zero) tensor components				
		Flexo-magnetic	Linear flexomagneto-electric	Linear magneto-electric	Piezo-magnetic	Piezo-electric
1	1	54	54	9	18	18
2	2	28	28	5	8	8
	$2'$	26	26	4	10	
m	m	26	26	4	8	10
	m'	28	28	5	10	
$mm2$	$m'm'2$	15	15	3	5	5
	$mm'2'$	13	13	2	3	
4	4	14	14	2	4	4
$4mm$	$4m'm'$	8	8	2	3	3
3	3	18	18	2	6	6
$3m$	$3m'$	11	11	1	2	4
6	6	12	12	2	4	4
$6mm$	$6m'm'$	7	7	2	3	3

The flexomagnetic and flexoelectric effects change the gradient terms in expressions (4.8) and (4.9); namely,

$$\begin{aligned}\tilde{g}^{(m)}_{klpn} &= g^{(m)}_{klpn} - Q^{(m)}_{ijkl} s_{ijsq} Q^{(m)}_{sqpn},\\ \tilde{g}^{(e)}_{klpn} &= g^{(e)}_{klpn} - Q^{(e)}_{ijkl} s_{ijsq} Q^{(e)}_{sqpn}.\end{aligned} \tag{4.11}$$

At the same time, the piezomagnetic and piezoelectric couplings renormalize the expansion coefficients in formulas (4.8) and (4.9):

$$\begin{aligned}\tilde{a}^{(m)}_{ij} &= a^{(m)}_{ij} - \frac{1}{2} d^{(m)}_{ilp} s_{lpkm} d^{(m)}_{jkm},\\ \tilde{a}^{(e)}_{ij} &= a^{(e)}_{ij} - \frac{1}{2} d^{(e)}_{ilp} s_{lpkm} d^{(e)}_{jkm}.\end{aligned} \tag{4.12}$$

In order to study the linear FMFE coupling in ferroelectrics-ferromagnets, let us consider a model for one-dimensional distributions of the one-component polarization and magnetization in an ultrathin nanotube with the internal radius R_i and the external radius R_o. The tube thickness $h = R_o - R_i$ is assumed to be very small as compared with the average tube radius $R = 0.5\,(R_o + R_i)$ (see Fig. 4.1, *a*). This simple model makes it possible to carry out analytical calculations for the average properties, which can be measured, by using the standard experimental methods. As an example, let us estimate the average gradient for thin tubes ($h \ll R$):

$$\begin{aligned}\overline{\frac{\partial P}{\partial x}\frac{\partial M}{\partial x}} &\approx \frac{1}{h}\int\limits_{R_i}^{R_o} \frac{\partial P\,(x)}{\partial x}\frac{\partial M\,(x)}{\partial x} dx \sim\\ &\sim \frac{2 r_e r_m \overline{MP}}{(r_e + r_m)\,(r_e + \Lambda_e)\,(r_m + \Lambda_m)\,h},\end{aligned} \tag{4.13}$$

where the electrical and magnetic correlation lengths are introduced as

$$r_e(T) = \sqrt{\frac{\tilde{g}^{(e)}}{\left|a^{(e)}_1(T)\right|}}, \quad r_m = \sqrt{\frac{\tilde{g}^{(m)}}{|K|}},$$

and $\Lambda_e = \tilde{g}^{(e)}/a^S$ and $\Lambda_m = \tilde{g}^{(m)}/K_S$ are the electric and magnetic extrapolation lengths, respectively. For ferroelectrics, the extrapolation length calculated from the first principles equals $\Lambda^e_k \approx 1$ nm [65]. Since the extrapolation length is proportional to the gradient coefficient, its renormalization due to the flexoeffect has also to be taken into account [64].

As follows from Eq. (4.13), the linear flexomagnetoelectric coupling induced by the surface stimulates an additional size dependence of the linear ME effect in nanosized multiferroics. The flexomagnetoelectric

coupling affects the magnetization and polarization distributions (see Figs.4.1, *b* and 4.1, *c*).

The energy of linear flexomagnetoelectric coupling that is typical of nanosystems and was calculated, by using the averaged expressions (4.13), looks like [64]

$$\overline{g^S_{\rm FME}} = \frac{1}{V}\int\limits_V g^S_{\rm FME} d^3r \approx$$

$$\approx s_u\left(\frac{2r_e r_m Q^{(m)}Q^{(e)}}{(r_e+r_m)(r_e+\Lambda_e)(r_m+\Lambda_m)} + \right.$$

$$\left. + \frac{r_m Q^{(m)} d^{(e)}}{(r_m+\Lambda_m)} + \frac{r_e Q^{(e)} d^{(m)}}{(r_e+\Lambda_e)}\right)\frac{\overline{MP}}{h}. \qquad (4.14)$$

In this formula, the tensor indices at the compliance, flexoeffect, piezomagnetic, and piezoelectric tensors are omitted to simplify the understanding. As one can see from Eq. (4.14) and Fig. 4.2, *a*, the flexomagnetoelectric coupling depends rather strongly on the system size. Namely, its value is reciprocal to the tube thickness h. The coupling magnitude decreases with the growth of extrapolation lengths Λ_m and Λ_e, because the gradients of order parameters decrease, as $\Lambda_{e,m}$ increases. For larger $\Lambda_{e,m}$, the linear flexomagnetoelectric coupling is smaller.

The following dimensionless parameters were introduced and used in numerical calculations:

$$\xi = \frac{Q^{(e)}_{44}Q^{(m)}_{44}}{c_{44}}\frac{M_0 P_0}{g^{(m)}}, \quad f = \frac{Q^{(e)}_{44}q^{(m)}_{44}}{c_{44}}\frac{P_0}{K r_m},$$

$$G_{em} \equiv \frac{\left|a^{(e)}_1(T)\right| P_0^2}{K\cdot M_0^2}, \quad P_0 = \sqrt{\frac{\left|a^{(e)}_1(T)\right|}{a^{(e)}_{11}}}. \qquad (4.15)$$

For ferromagnetic bulk materials, M_0 is the spontaneous magnetization, P_0 the temperature-dependent spontaneous polarization of a bulk material at $a^{(e)}_1(T) < 0$ (intrinsic ferroelectric) or a certain characteristic polarization of the material at $a^{(e)}_1(T) > 0$ (extrinsic ferroelectric), ξ is the dimensionless linear coefficient of flexomagnetoelectric coupling proportional to $Q^{(e)}_{44}Q^{(m)}_{44}$, f the dimensionless nonlinear coefficient of flexomagnetoelectric coupling proportional to $Q^{(e)}_{44}q^{(m)}_{44}$, and G_{em} the ratio between the polarization and magnetization energies. At temperatures far from the bulk ferroelectric and magnetic transitions (Curie or Neél), the magnitudes of those parameters

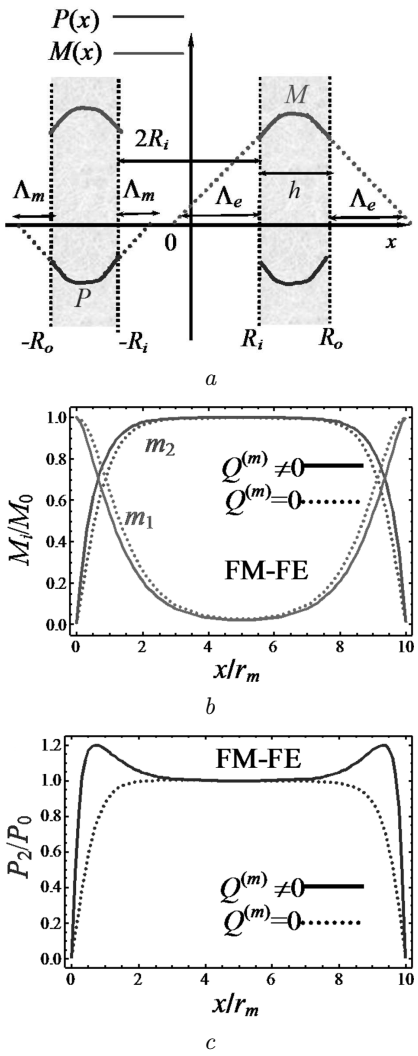

Fig. 4.1. One-dimensional distributions of the polarization and magnetization (solid curves) in a nanotube; Λ_e and Λ_m are the corresponding extrapolation lengths, i.e. the distances along the axis X confined by the tangent lines drawn from the points $x = \pm R_{i,o}$ (*a*). The spontaneous magnetization $M_{1,2}(x)$ (*b*) and spontaneous polarization $P_2(x)$ (*c*) in a ferromagnet-ferroelectric nanotube. The solid curve $P_2(x)$ and the dashed curve $P_1(x)$ were obtained in the cases where the flexomagnetic effect exists ($Q^{(m)} \neq 0$) or not ($Q^{(m)} = 0$), respectively. The dashed curve $P_1(x)$ was obtained in the case without the flexomagnetic effect ($Q^{(m)} = 0$). The extrapolation lengths Λ_e and Λ_m equal zero (Reproduced from [64], with the permission of AIP Publishing)

are as follows: $\xi \approx 10^{-6}\div 10^{-1}$, $f \approx 10^{-6}\div 10^{-2}$, $G_{em} \approx 0.1\div 10$, $P_0 \approx 0.1\div 1$ C/m^2 for the extrinsic ferroelectric and $0.01\div 0.1$ C/m^2 for the intrin-

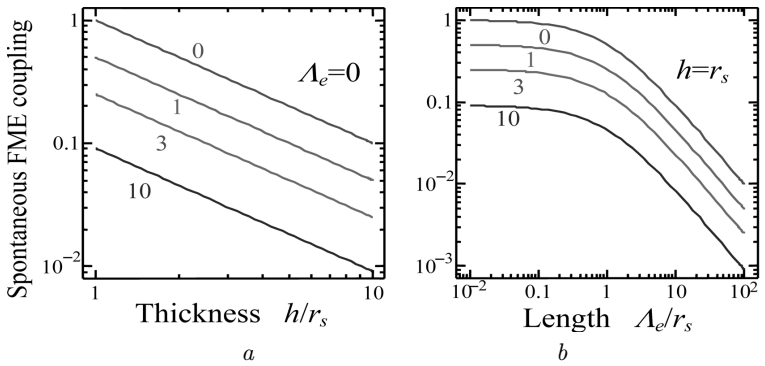

Fig. 4.2. Dependences of the relative flexomagnetoelectric effect coefficients $\frac{g^S_{\rm FME}}{Q^{(m)}{}_{s_u}Q^{(e)}}$ on the nanotube thickness h (a) and the extrapolation magnetization length Λ_m (b). The characteristic length $r_S = \frac{2r_e r_m}{(r_e+r_m)}$. The curves correspond to various values of the ratio Λ_m/r_m (indicated near the curves). The other parameters are (a) $d^{(e)} = 0$, $d^{(m)} = 0$, $\Lambda_e/r_e = 0$ and (b) $h = r_S$ (Reproduced from [64], with the permission of AIP Publishing)

sic ferroelectric. The electric and magnetic correlation lengths equal

$$r_e(T) = \sqrt{\frac{\tilde{g}^{(e)}}{\left|a_1^{(e)}(T)\right|}}, \quad r_m\,(T) = \sqrt{\frac{\tilde{g}^{(m)}}{|K\,(T)|}}. \qquad (4.16)$$

Those lengths vary within the intervals $r_e(T) \approx \approx 0.5 \div 5$ nm and $r_m(T) \approx 1 \div 10$ nm. The values of the parametersfor numerical calculations were selected according to the estimates of parameters (4.16).

It is worth emphasizing that the linear flexomagnetoelectric energy described by expression (4.14) may appear in bulk inhomogeneous systems with the externally induced non-zero flexomagnetic effect.

4.3. Linear flexomagnetoelectric coupling in nanosized antiferromagnets-ferroelectrics

Below, we consider ferroelectrics-antiferromagnets with two sublattices a and b. The antiferromagnetic order parameter $\mathbf{L} = \left(\mathbf{M}^{(a)} - \mathbf{M}^{(b)}\right)/2$ is transformed as a pseudovector at symmetry operations applied to each sublattice and changes its sign at the $a \leftrightarrow b$ operation. The sign of the piezomagnetic effect is known [66] to be determined by the sign of $\mathbf{L}$. This means that the non-zero components of the piezomagnetic tensor $d^{(m)}_{ijk}$ determine the contribution $d^{(m)}_{ijk} L_i u_{jk}$ or $\tilde{d}^{(m)}_{ijk} H_i u_{jk}$ to the free energy. The contributions from the linear magnetoelectric effect can be written in the form $Q^{(m)}_{ijkl}\frac{\partial u_{ij}}{\partial x_k} L_l$ or $\tilde{Q}^{(m)}_{ijkl}\frac{\partial u_{ij}}{\partial x_k} H_l$. They are linear in $\mathbf{L}$.

Below, the magnetic field $\mathbf{H}$ and the electric field $\mathbf{E}$ are assumed to be absent. Therefore, the ferromagnetic order parameter $\mathbf{M} = \left(\mathbf{M}^{(a)} + \mathbf{M}^{(b)}\right)/2$ is also absent, and the free energy components of a spatially confined antiferromagnet look like [64]

$$F_V = \int\limits_V (g_{\rm FE} + g_{\rm AFM} + \\ + g_{\rm elast} + g_{\rm striction} + g_{\rm flexo}) d^3 r, \qquad (4.17)$$

$$F_S = \int\limits_S d^2 r \left(\frac{a_i^S}{2} P_i^2 + \left(2K_S - \tilde{K}_S\right)(\mathbf{Ln})^2\right), \qquad (4.18)$$

where $\mathbf{n}$ is a normal to the surface, K_S the surface intralattice anisotropy, and $\tilde{K}_S$ the surface interlattice anisotropy [67, 68]; the ferroelectric contribution $g_{\rm FE}$ is expressed by formula (4.8) at $\mathbf{E} = 0$. The antiferromagnetic contribution to the free energy equals

$$g_{\rm AFM} = -J \cdot \mathbf{L}^2 + \left(2K - \tilde{K}\right) L_3^2 + \\ + \left(g^{(m)}_{ijkl} - \tilde{g}^{(m)}_{ijkl}\right) \frac{\partial L_i}{\partial x_j} \frac{\partial L_k}{\partial x_l}, \qquad (4.19)$$

where $g^{(m)}_{ijkl}$ and $\tilde{g}^{(m)}_{ijkl}$ are components of the intra- and interlattice inhomogeneous exchange tensors, respectively; K and $\tilde{K}_S$ the intra- and interlattice bulk anisotropies, respectively; and J the intralattice exchange interaction constant. The condition $J > 0$ is necessary for the antiferromagnetic state to exist, with the equality $\mathbf{M}^{(a)} = -\mathbf{M}^{(b)}$ being valid in zero and low magnetic fields.

The elastic contribution g_{elast} to the free energy is described by formula (4.10). The piezoelectric, piezomagnetic, electro-, and magnetostriction contributions equal

$$g_{\text{striction}} = \left(-d_{ijk}^{(e)} P_i u_{jk} - d_{ijk}^{(m)} L_i u_{jk} - q_{ijkl}^{(e)} u_{ij} P_k P_l - \right.$$

$$\left. - \left(2q_{ijkl}^{(m)} - \tilde{q}_{ijkl}^{(m)}\right) u_{ij} L_k L_l\right), \tag{4.20}$$

where $q_{ijkl}^{(m)}$ are components of the sublattice electrostriction tensor, and $\tilde{q}_{ijkl}^{(m)}$ are components of the interlattice bulk electrostriction tensor. The flexomagnetic and flexoelectric energies equal

$$g_{\text{flexo}} = \frac{Q_{ijkl}^{(m)}}{2}\left(\frac{\partial u_{ij}}{\partial x_k} L_l - u_{ij}\frac{\partial L_l}{\partial x_k}\right) +$$

$$+ \frac{Q_{ijkl}^{(e)}}{2}\left(\frac{\partial u_{ij}}{\partial x_k} P_l - u_{ij}\frac{\partial P_l}{\partial x_k}\right). \tag{4.21}$$

Unlike the free energy of ferroelectrics-ferromagnets, which was considered in the previous section, we now discuss ferroelectrics-ferromagnets with a definite symmetry. We assume that, near the surface, the surface symmetry group is $4m'm'$ at high temperatures, which corresponds to the $m'3m'$ bulk symmetry group and allows both the flexomagnetic and linear ME couplings to exist. Let us consider the case where the components P_1 of cferroelectric polarization, two components $L_{1,3}$ of the vector of antiferromagnetic order parameter, and the magnetic anisotropy axis are directed along the z-axis (Fig. 4.3, *a*).

Below, we consider ultrathin antiferromagnetic-ferroelectric films on a substrate that provides a negligibly small misfit deformation at the film-substrate interface. In this case, $u_{11} = u_{22} = u_{23} = 0$ and $\sigma_{13} = \sigma_{23} = \sigma_{33} = 0$, i.e.

$$u_{33} = \frac{1}{c_{11}}\left(q_{12}^{(e)} P_1^2 + d_{33}^{(m)} L_3 + \right.$$

$$\left. + \left(2q_{11}^{(m)} - \tilde{q}_{11}^{(m)}\right) L_3^2 + Q_{11}^{(m)}\frac{\partial L_3}{\partial x_3}\right), \tag{4.22a}$$

$$u_{13} = \frac{1}{c_{44}}\left(d_{15}^{(e)} P_1 + Q_{44}^{(e)}\frac{\partial P_1}{\partial x_3} + d_{15}^{(m)} L_1 + \right.$$

$$\left. + \left(2q_{44}^{(m)} - \tilde{q}_{44}^{(m)}\right) L_1 L_3 + Q_{44}^{(m)}\frac{\partial L_1}{\partial x_3}\right). \tag{4.22b}$$

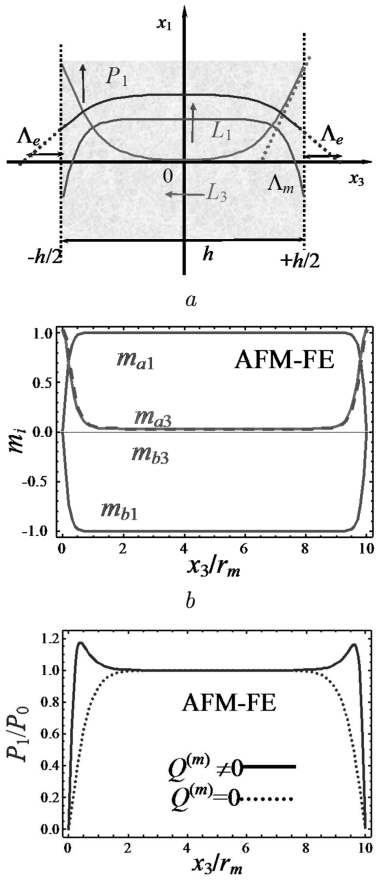

Fig. 4.3. One-dimensional distributions of the antiferromagnetic order parameter L and the polarization P inside the film (*a*). Non-uniform distributions of the normalized sublattice magnetizations $m_{a1,3}(x_3) = M_{a1,3}(x_3)/M_0$, $m_{b1,3}(x_3) = M_{b1,3}(x_3)/M_0$ (*b*), and the polarization $P_1(x)$ in an antiferromagnetic-ferroelectric film (*c*). The antimagnetization components are $L_1 = M_0(m_{a1} - m_{b1})/2$ and $L_3 = M_0(m_{a3} - m_{b3})/2$. The solid and dashed curves $P_1(x)$ were obtained in the cases where the flexomagnetic effect is present ($Q^{(m)} \neq 0$) or absent ($Q^{(m)} = 0$), respectively. The dashed and solid curves for the magnetization practically coincide (*b*). Λ_e and Λ_m are extrapolation lengths. The dimensional parameters are $\xi = 0$ (dotted curves) and -0.2 (solid curves), $f = 0.01$, $G_{em} = 0.5$, $r_e/r_m = 0.5$, and $a_1^{(e)}(T) < 0$. The extrapolation length equals zero (Reproduced from [64], with the permission of AIP Publishing)

By substituting strains (4.22) into the free energy and performing the Legendre transformation, we arrive at the following expression for the free energy:

$$\tilde{F} = \int\limits_V \left(\tilde{g}_{\text{FE}} + \tilde{g}_{\text{AFM}} + \tilde{g}_{\text{ME}} + \tilde{g}_{\text{FME}}\right) d^3 r +$$

$$+\int\limits_S d^2r\left(\frac{a_i^S}{2}P_i^2+\left(2K_S-\tilde{K}_S\right)(\mathbf{nL})^2\right). \quad (4.23)$$

The ferroelectric component of the free energy acquires the form

$$\tilde{g}_{\rm FE}=\frac{1}{2}\left(a_1^{(e)}-\frac{\left(d_{15}^{(e)}\right)^2}{c_{44}}\right)P_1^2+\left(\frac{a_{11}^{(e)}}{4}-\frac{(q_{12}^{(e)})^2}{2c_{11}}\right)P_1^4+$$
$$+...+\left(\frac{g_{44}^{(e)}}{2}-\frac{\left(Q_{44}^{(e)}\right)^2}{2c_{44}}\right)\left(\frac{\partial P_1}{\partial x_3}\right)^2. \quad (4.24)$$

For the $4m'm'$ symmetry, the antiferromagnetic contribution to the free energy equals

$$\tilde{g}_{\rm AFM}=\left(-J(L_1^2+L_3^2)+\left(2K-\tilde{K}-\frac{(d_{33}^{(m)})^2}{2c_{11}}\right)L_3^2-\right.$$
$$-\frac{\left(2q_{44}^{(m)}-\tilde{q}_{44}^{(m)}\right)Q_{44}^{(m)}}{c_{44}}L_1L_3\frac{\partial L_1}{\partial x_3}-\frac{d_{33}^{(m)}Q_{11}^{(m)}}{c_{11}}\times$$
$$\times L_3\left(\frac{\partial L_3}{\partial x_3}\right)+\left(g_{44}^{(m)}-\tilde{g}_{44}^{(m)}-\frac{\left(Q_{44}^{(m)}\right)^2}{2c_{44}}\right)\left(\frac{\partial L_1}{\partial x_3}\right)^2+$$
$$+\left(g_{11}^{(m)}-\tilde{g}_{11}^{(m)}-\frac{\left(Q_{11}^{(m)}\right)^2}{2c_{11}}\right)\left(\frac{\partial L_3}{\partial x_3}\right)^2-$$
$$\left.-\frac{d_{15}^{(m)}Q_{44}^{(m)}}{c_{44}}L_1\frac{\partial L_1}{\partial x_3}\right). \quad (4.25)$$

The contribution of the ME coupling to the free energy,

$$\tilde{g}_{\rm ME}=-\frac{d_{15}^{(e)}d_{15}^{(m)}}{c_{44}}P_1L_1-\frac{q_{12}^{(e)}d_{33}^{(m)}}{c_{11}}P_1^2L_3-$$
$$-\frac{\left(2q_{44}^{(m)}-\tilde{q}_{44}^{(m)}\right)d_{15}^{(e)}}{c_{44}}P_1L_1L_3-$$
$$-\frac{q_{12}^{(e)}\left(2q_{11}^{(m)}-\tilde{q}_{11}^{(m)}\right)}{c_{11}}P_1^2L_3^2, \quad (4.26)$$

contains a new term associated with the flexomagnetoelectric coupling,

$$\tilde{g}_{\rm FME}=\frac{1}{c_{44}}\left(-Q_{44}^{(e)}Q_{44}^{(m)}\frac{\partial L_1}{\partial x_3}\frac{\partial P_1}{\partial x_3}-Q_{44}^{(e)}d_{15}^{(m)}L_1\frac{\partial P_1}{\partial x_3}-\right.$$
$$-d_{15}^{(e)}Q_{44}^{(m)}\frac{\partial L_1}{\partial x_3}P_1+Q_{44}^{(e)}\left(\tilde{q}_{44}^{(m)}-2q_{44}^{(m)}\right)\left(\frac{\partial P_1}{\partial x_3}\right)L_1L_3-$$
$$\left.-\frac{q_{12}^{(e)}Q_{11}^{(m)}}{c_{11}}P_1^2\frac{\partial L_3}{\partial x_3}\right). \quad (4.27)$$

Note that new linear and nonlinear terms can appear in expression (4.27) in the case of ferroelectrics-antiferromagnets with the increasing of the polarization P gradient and/or the antiferromagnetic order parameter L gradient. The flexomagnetolectric coupling affects the spatial distribution of the order parameter, as is shown in Figs. 4.3, *b* and *c*. In particular, there appear pronounced maxima in the polarization distribution plot, in the sections, where the gradient of L takes place, i.e. near the film surface, where L_1 and L_3 change their values owing to the rotation of the vector L.

For a thin film with thickness h, we calculated the average values

$$\overline{\left(\frac{\partial P_1}{\partial x}\right)\left(\frac{\partial L_1}{\partial x}\right)}=\frac{1}{h}\int\limits_{-h/2}^{-h/2}\frac{\partial P_1(x)}{\partial x}\frac{\partial L_1(x)}{\partial x}dx\approx$$
$$\approx\frac{2r_er_m\overline{P_1L_1}}{(r_e+r_m)(r_e+\Lambda_e)(r_m+\Lambda_m)h}, \quad (4.28a)$$
$$\overline{\left(\frac{\partial P_1}{\partial x}\right)L_1L_3}=\frac{1}{h}\int\limits_{-h/2}^{-h/2}\frac{\partial P_1(x)}{\partial x}L_1(x)L_3(x)dx\approx$$
$$\approx\frac{r_e\overline{P_1L_1L_3}}{(r_e+\Lambda_e)h}. \quad (4.28b)$$

Using the mean values (4.28), we obtained that the spontaneous linear flexomagnetoelectric coupling gives rise to the following additional energy in nanosystems:

$$\overline{g_{\rm FME}^S}=\frac{1}{V}\int\limits_V g_{\rm FME}^S d^3r\sim$$
$$\sim\frac{1}{hc_{44}}\left(\frac{-2r_er_m\overline{P_1L_1}Q_{44}^{(e)}Q_{44}^{(m)}}{(r_e+r_m)(r_e+\Lambda_e)(r_m+\Lambda_m)}-\right.$$
$$-Q_{44}^{(e)}d_{15}^{(m)}\frac{r_e\overline{P_1L_1}}{(r_e+\Lambda_e)}-Q_{44}^{(e)}d_{15}^{(m)}\frac{r_m\overline{P_1L_1}}{(r_m+\Lambda_m)}+$$
$$\left.+Q_{44}^{(e)}\left(\tilde{q}_{44}^{(m)}-2q_{44}^{(m)}\right)\frac{r_e\overline{P_1L_1L_3}}{(r_e+\Lambda_e)}\right). \quad (4.29)$$

As one can see from Eq. (4.29), the flexomagnetoelectric energy strongly depends on the film thickness h,

being inversely proportional to this parameter. One can also see that the influence of the flexomagnetoelectric effect decreases, as the film thickness h or the extrapolation length increases.

As was done for spatially confined bulk antiferromagnets-ferroelectrics, in order to generalize the results discussed above onto the case of other symmetry, all classes of antiferromagnets-ferroelectrics with $Q^{(m)}_{ijkl} \neq 0$ were determined [64].

4.4. Influence of flexomagnetoelectric coupling on susceptibility

Let a thin antiferroelectric film of the $4m'm'$ symmetry be subjected to the action of external magnetic, **H**, and electric, **E**, fields in the geometry shown in Fig. 4.4, *a* (the magnetic anisotropy axis is directed along the axis x_3). The expressions for the ferromagnetic and antiferromagnetic order parameters look like $\mathbf{M} = \left(\mathbf{M}^{(a)} + \mathbf{M}^{(b)}\right)/2$ and $\mathbf{L} = \left(\mathbf{M}^{(a)} - \mathbf{M}^{(b)}\right)/2$, respectively. Using the solutions of elasticity theory in the linear approximation, we can exclude non-trivial strain components from the free energy functional making use of the Legendre transformation and obtain the following expression for the renormalized free energy [64]:

$$\tilde{F}_V = \int\limits_V \left(\tilde{g}_{\rm FE} + \tilde{g}_{\rm AFM} + \tilde{g}_{\rm ME} + \tilde{g}_{\rm FME}\right) d^3r, \tag{4.30a}$$

$$\tilde{F}_S = \int\limits_S d^2r \Bigg(\frac{a^S_i}{2} P_i^2 + \left(2K_S + \tilde{K}_S\right)(\mathbf{Mn})^2 + \\ + \left(2K_S - \tilde{K}_S\right)(\mathbf{nL})^2\Bigg), \tag{4.30b}$$

where the ferroelectric component equals

$$\tilde{g}_{\rm FE} = \frac{a^{(e)}_1(T)}{2} P_1^2 + \left(\frac{a^{(e)}_{11}}{4} - \frac{\left(q^{(e)}_{12}\right)^2}{2c_{11}}\right) P_1^4 + ... + \\ + \left(\frac{g^{(e)}_{44}}{2} - \frac{\left(Q^{(e)}_{44}\right)^2}{2c_{44}}\right)\left(\frac{\partial P_1}{\partial x_3}\right)^2 - P_1 E_1, \tag{4.31}$$

and the antiferromagnetic component equals

$$\tilde{g}_{\rm AFM} = J\left(\mathbf{M}^2 - \mathbf{L}^2\right) - 2\left(\mathbf{H}\,\mathbf{M}\right) + 2K\left(M_3^2 + L_3^2\right) + \\ + \tilde{K}\left(M_3^2 - L_3^2\right) + 2\left(\frac{g^{(m)}_{44}}{2} - \frac{\left(Q^{(m)}_{44}\right)^2}{2c_{44}}\right) \times \\ \times \left(\left(\frac{\partial M_1}{\partial x_3}\right)^2 + \left(\frac{\partial L_1}{\partial x_3}\right)^2\right) + 2\left(\frac{g^{(m)}_{11}}{2} - \frac{\left(Q^{(m)}_{11}\right)^2}{2c_{11}}\right) \times \\ \times \left(\left(\frac{\partial M_3}{\partial x_3}\right)^2 + \left(\frac{\partial L_3}{\partial x_3}\right)^2\right) + \left(\tilde{g}^{(m)}_{44} - \frac{\left(Q^{(m)}_{44}\right)^2}{c_{11}}\right) \times \\ \times \left(\left(\frac{\partial M_1}{\partial x_3}\right)^2 - \left(\frac{\partial L_1}{\partial x_3}\right)^2\right) + \left(\tilde{g}^{(m)}_{11} - \frac{\left(Q^{(m)}_{11}\right)^2}{c_{11}}\right) \times \\ \times \left(\left(\frac{\partial M_3}{\partial x_3}\right)^2 - \left(\frac{\partial L_3}{\partial x_3}\right)^2\right). \tag{4.32}$$

The condition $J > 0$ has to be satisfied for the antiferromagnetic state ($\mathbf{M} = 0$, $\mathbf{L} \neq 0$) to be stable in the zero magnetic field. On the other hand, the condition $J < 0$ is necessary for the ferromagnetic state ($\mathbf{L} = 0$, $\mathbf{M} \neq 0$) to be stable in arbitrary magnetic fields.

The magnetoelectric and flexomagnetoelectric components of the free energy equal

$$\tilde{g}_{\rm ME} = 2f_{11}M_1P_1 + 2w_{111}M_1P_1^2 - 2\frac{q^{(e)}_{12}q^{(m)}_{11}}{c_{11}} \times \\ \times P_1^2\left(M_3^2 + L_3^2\right) - \frac{q^{(e)}_{12}\tilde{q}^{(m)}_{11}}{c_{11}} P_1^2\left(M_3^2 - L_3^2\right) \tag{4.33}$$

and

$$\tilde{g}_{\rm FME} = \Bigg(-2\frac{q^{(e)}_{12}Q^{(m)}_{11}}{c_{11}} P_1^2 \frac{\partial M_3}{\partial x_3} - \\ - 2Q^{(m)}_{44}\frac{Q^{(e)}_{44}}{c_{44}}\frac{\partial P_1}{\partial x_3}\frac{\partial M_1}{\partial x_3} - \frac{Q^{(e)}_{44}}{c_{44}} d^{(m)}_{15} M_1 \frac{\partial P_1}{\partial x_3} - \\ - d^{(e)}_{15}\frac{Q^{(m)}_{44}}{c_{44}} P_1 \frac{\partial M_1}{\partial x_3} - 2\frac{Q^{(e)}_{44}}{c_{44}}\left(\frac{\partial P_1}{\partial x_3}\right) \times \\ \times \left(\left(q^{(m)}_{44} + \tilde{q}^{(m)}_{44}\right) M_1M_3 + \left(q^{(m)}_{44} - \tilde{q}^{(m)}_{44}\right) L_1L_3\right)\Bigg), \tag{4.34}$$

respectively. Attention should be paid to that the terms quadratic in the magnetization vector, $\sim M_iM_j\frac{\partial P_k}{\partial x_l}$ and $\sim L_iL_j\frac{\partial P_k}{\partial x_l}$, are relevant to all materials, because the flexoelectric, $Q^{(e)}_{ijkl}$, and magnetostriction, $q^{(m)}_{ijnp}$, tensors have non-zero components at an arbitrary symmetry. The terms linear in the magnetization vector, $\sim\frac{\partial P_1}{\partial x_3}\frac{\partial M_1}{\partial x_3}$ and $\sim P_1^2\frac{\partial M_3}{\partial x_3}$, appear in the free energy, if the magnetic fields are

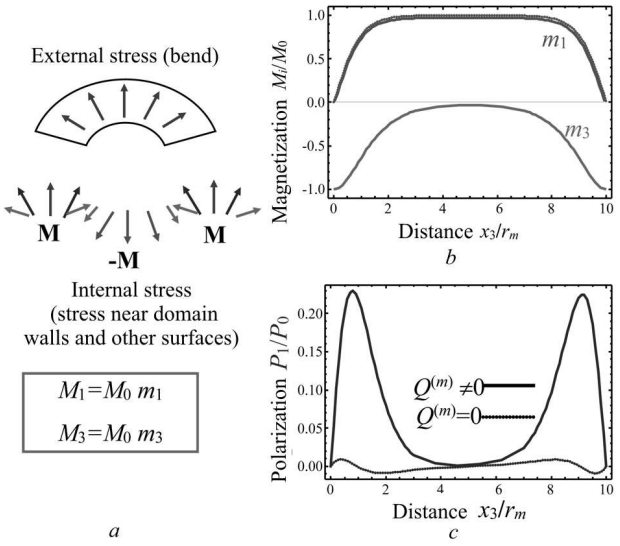

Fig. 4.4. Scheme of the non-homogeneous external stress (bend) and the internal stress (e.g., near the domain walls of an object or other possible surfaces), which cause the flexomagnetic effect in ferromagnetics (a), non-homogeneous normalized components of the nagnetization $m_{1,3}(x_3) = M_{1,3}(x_3)/M_0$ induce the polarization $P_1(x_3)$ in ferromagnetics (b). The solid curve $P_1(x_3)$ is obtained in the case where the flexomagnetic effect exists $Q(m) \neq 0$. Dotted lines of the polarization correspond to the case without flexomagnetic effect $Q(m) = 0$. The dimensionless parameters are as follows: $\xi = 0, -0.1$ (пунктирні і суцільні лінії відповідно) $f = 0.01$, $G_{em} = 0.2$, $r_e/r_m = 0.5$, and $a_1^{(e)}(T) > 0$. The extrapolation length equals zero. (Reproduced from [64], with the permission of AIP Publishing)

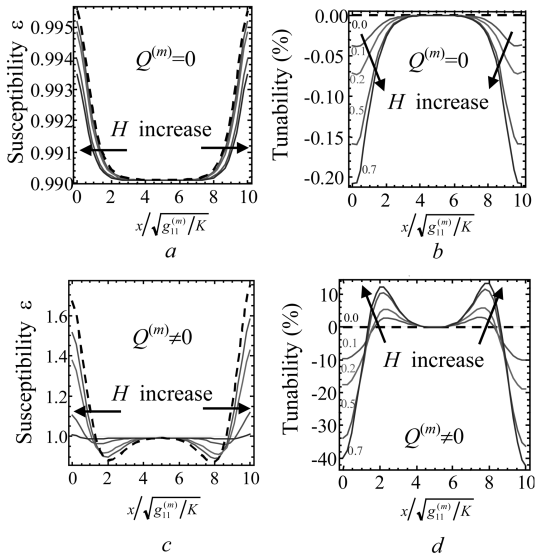

Fig. 4.5. Dependences of the linear dielectric constant (a, b) and magnetoelectric susceptibility (c, d) on the relative magnetic field magnitude $H/(MK) = 0$, 0.1, 0.2, 0.5, and 0.7 (indicated near the curves) in the cases with no flexomagnetic effect (a, b) and with it (c, d). The dotted curves correspond to the zero magnetic field. The dimensional parameter $\xi = 0$ (dashed curves) and -0.2 (solid curves), $f = 0.01$, $G_{em} = 0.5$, $r_e/r_m = 0.5$, and $a_1^{(e)}(T) > 0$ (Reproduced from [64], with the permission of AIP Publishing)

higher than the critical value of the spin-flop phase transition in an antiferromagnetic nanomaterial with the non-zero flexomagnetic effect ($Q_{ijkl}^{(m)} \neq 0$).

The free energy (4.30) can be used to describe a number of different cases; namely,

• $\mathbf{L} \neq 0$ and $\mathbf{M} = 0$ in the magnetic fields below the critical one; in this case, $\mathbf{P}$ and $\mathbf{L}$ are non-zero;

• $\mathbf{L} \neq 0$ and $\mathbf{M} \neq 0$ for the magnetic fields above the critical one, but lower than the spin-flop transition field; in this case, $\mathbf{P}$, $\mathbf{L}$, and $\mathbf{M}$ are non-zero;

• $\mathbf{L} \neq 0$ and $\mathbf{M} \neq 0$ for the ferromagnetic phase in a strong magnetic field above the spin-flop phase-transition value; in this case, $\mathbf{P}$ and $\mathbf{M}$ are non-zero.

Experimental methods [34] are applied mostly often to study the magnetoelectric properties of a material, its dielectric constant and magnetoelectric susceptibility. The average magnetization, polarization, linear dielectric permeability in various magnetic fields, and magnetoelectric susceptibility can be calculated from the free energy functional. The dependences of the dielectric constant and the magnetoelectric susceptibility on the magnetic field are shown in Fig. 4.5. One can see that the flexomagnetoelectric coupling between the polarization and magnetization substantially affects the susceptibility and dielectric permeability. In particular, in the absence of flexoeffects, the susceptibility by means of the quadratic ME coupling cannot exceed 1% (Fig. 4.5, b), whereas the flexomagnetoelectric coupling results in the susceptibility change by 10–30% (Fig. 4.5, c).

5. Size Effect of the Magnetoelectric Coupling in Bismuth Ferrite Nanoparticles

Bismuth ferrite ($BiFeO_3$) is one of the most promising multiferroics with rather high ferroelectric and antiferromagnetic transition temperatures, as well as

a relatively high ME coupling coefficient at room temperature. Thus, bismuth ferrite is quite sensitive to the influence of external electric and magnetic fields. In this section, the influence of the size of semiellipsoidal $BiFeO_3$ nanoparticles attached to a rigid substrate on the phase diagram and the FE and ME properties is considered. The spatial distribution of the spontaneous polarization vector in a nanoparticle, the phase diagram, and the paramagnetoelectric (PME) coefficient were calculated in the framework of the Landau–Ginzburg–Devonshire (LGD) theory. The analytical expressions were derived for the dependences of the ferroelectric transition temperature, the average polarization, the linear dielectric susceptibility, and the PME coefficient on the particle size in the general case of a semiellipsoidal nanoparticle with three different semiaxes a, b, and c (height). The analysis of the results obtained testifies that the phase diagrams, the spontaneous polarization, and the PME coefficient are very sensitive to the ratio between the particle sizes in the polarization direction and are less sensitive to the size magnitudes *per se*.

5.1. $BiFeO_3$ multiferroic in fundamental researches

Multiferroics, which are characterized by two or more long-range order parameters, are perfect systems for fundamental researches of the relation between the ferroelectric polarization, structural antiferrodistortion, and antiferromagnetic order parameter [69–72]. This relation is responsible for the unique physical properties of multiferroics [73]. For example, the biquadratic and linear ME couplings result in an impressive effect known as the giant megnetoelectric effect in multiferroics [74]. The biquadratic coupling between the structural, polarization, and dielectric order parameters was considered in works [75–77]. It is responsible for an unusual behavior of the physical properties of ferroelastics, quantum paraelectrics. The linear-quadratic PME effect has to exist in the paramagnetic phase of ferroics at a temperature below the paraelectric-ferroelectric phase-transition one, where the electric polarization differs from zero. This effect was observed in $NiSO_4 \cdot 6H_2O$ [78], Mn-doped $SrTiO_3$ [79], $Pb(Fe_{1/2}\ Nb_{1/2})O_3$ [80–82], and $Pb(Fe_{1/2}Nb_{1/2})O_3$-$PbTiO_3$ solid solution [83]. Note that the PME effect can be expected to take place in many nanosized ferroics that become paramagnetic at the temperature elevation owing to the induced transition from the ferromagnetic or antiferromagnetic phase.

$BiFeO_3$ is one of the most interesting multiferroics with a strong ferroelectric polarization, antiferromagnetism at room temperature, and enhanced electric transport along the domain walls. [84–89]. Bulk $BiFeO_3$ is antiferrodistortive at temperatures below 1200 K. This is a ferroelectric with a high spontaneous polarization below 1100 K and an antiferromagnet below the Neél temperature $T_N \approx 650$ K [90, 91]. Well-pronounced multiferroic properties were observed in $BiFeO_3$ thin films and heterostructures [30, 92–95]. There are a lot of experimental and theoretical studies concerning the physical properties of bulk $BiFeO_3$ and $BiFeO_3$ thin films [68, 77–79, 96–102]. Nevertheless, plenty of other important issues concerning the appearance of the polarization, magnetic, and other electrophysical properties of $BiFeO_3$ nanoparticles remained practically beyond the scope of researches [103, 104].

5.2. Multiferroic nanoparticles. The state of art

According to modern requirements to the miniaturization of the nanotechnology for a storage of the information packed to super-high densities in nonvolatile memory cells, it is very important that the nanoparticle size in self-ordered arrays should be diminished without substantial worsening of their ME properties. A promising example of the preservation of polar and dielectric properties of a material is the application of ferroelectric nanoparticles of various modifications. In particular, Yadlovker and Berger [105–107] reported unexpected experimental results concerning the enhancement of polar properties in cylindrical nanoparticles of Rochelle salt. Frey and Payne [108], Zhao *et al.* [109], and Erdem *et al.* [110] demonstrated a possibility to control the temperature of a ferroelectric phase transition, as well as the magnitude and position of a dielectric permittivity maximum, for $BaTiO_3$ and $PbTiO_3$ nanopowders and nanoceramics. The research of $KTa_{1-x}Nb_xO_3$ nanopowders [111] and ceramic nanograins [112–114]

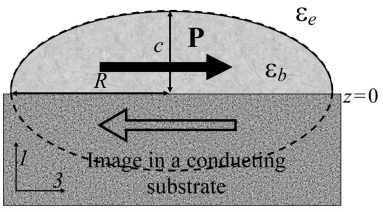

Fig. 5.1. Semiellipsoidal uniformly polarized ferroelectric nanoparticle attached to a conductive substrate (e.g., Pt). The one-component ferroelectric polarization is directed along the X-axis. The semiellipsoid height is equal to c; the lateral semiaxes to a and b (Adapted from [128], with the permission of AIP Publishing)

revealed the emergence of new polar phases and a shift of the phase transition temperature with respect to that in bulk crystals. The size effects were detected in $SrBi_2Ta_2O_9$ nanoparticles by Yu *et al.* [115] and Ke *et al.* [116], by using Raman spectroscopy.

The list of experimental results can be continued. Therefore, new theoretical researhes of ferroelectric nanoparticles are important from the viewpoint of both the fundamental science and the technological applications. In particular, the influence of the surface and confinement effects on the phase diagrams, the polar and electrophysical properties of $BiFeO_3$ nanoparticles have not been studied enough. Such a research can be very useful for the science itself and for advanced applications, because the theory of size effects in nanoparticles allows us to determine the physical origin of polar and other anomalies in physical properties, the change in the temperature of a phase transition in nanoparticles with a decrease of their size. In particular, by using the phenomenological approach, Niepce [117], Huang *et al.* [118, 119], Ma [120], Eliseev *et al.* [50], and Morozovska *et al.* [11, 121–124] showed that the transition temperature variations and the enhancement or weakening of polar properties in spherical and cylindrical nanoparticles are governed by various physical mechanisms, such as the correlation effect, depolarization fields, flexolectricity, electrostriction, and surface tension.

5.3. Motivation and formulation of the problem

Semiellipsoidal nanoparticles can be considered as a model for studying the influence of size effects on the physical properties of ferrite nanoislands. $BiFeO_3$ nanoislands and their self-ordered arrays can be formed on anisotropic substrates making use of various methods [125–127]. The particles usually possess different axial sizes in the substrate plane owing to the anisotropy of the substrate conductivity. Recent progress in the production technology of such nanoparticles made the synthesis of nanoparticles that are currently used to manufacture microdrives, microwave phase shifter, infrared sensors, transistors, energy-collecting devices, and others economically efficient. The mechanism of correlation between the sizes, geometry, and physical parameters of nanoparticles, as well as the related phenomena, such as spontaneous polarization, antiferromagnetic and antiferrodistortive ordering, the width of domain walls, and the stability of domains, must be studied experimentally and simulated theoretically. Among of the most important fundamental tasks to be solved, there are the evaluation of the polarization stability limit and the study of the mechanisms that govern the domain wall motion and the polarization switching in nano-scaled volumes.

All that stimulated us to study the influence of size effects on the FE, AFE, and ME properties of semiellipsoidal $BiFeO_3$ nanoparticles theoretically, in the framework of the Landau–Ginzburg–Devonshire approach, classical electrostatics, and elasticity theory [128]. Ferroelectricity is known to be a phenomenon associated with the long-range ordering of dipole moments. This ordering is characterized by a certain transition temperature, which depends on some factors such as the size, material, structural homogeneity, and so forth. The size effects are assumed to be connected with either internal (mainly, this is the atomic polarization) or external (stresses, microstructure, polarization, screening, and others) factors.

Let us consider ferroelectric nanoparticles in the form of semiellipsoidal islands, which were deposited onto a rigid conductive substrate. An ellipsoid is characterized by different values of its semiaxis lengths a, b, and c measured along the axes X, Y, and Z, respectively. Let ε_b and ε_e denote the dielectric permittivity inside and outside the ferroelectric nanoparticle, respectively. A one-component ferroelectric polarization in the particle is directed along the crystallographic axis 3, i.e. in parallel to the interface $z = 0$ (Fig. 5.1).

Let us assume that the dependence of the longitudinal components "1" and "2" (in the crystallographic coordinate system) of the electric polar-

ization on the internal electric field $\mathbf{E}^i$ is linear, i.e. $P_1 = \varepsilon_0 \left(\varepsilon_b^i - 1\right) E_1^i$ and $P_2 = \varepsilon_0 \left(\varepsilon_b^i - 1\right) E_2^i$, where $\varepsilon_0 = 8.85 \times 10^{12}$ F/m is the universal dielectric constant (the dielectric permittivity of vacuum) and the isotropic background dielectric constant ε_b^i is relatively small $\left(\varepsilon_b^i \leq 10\right)$ [129]. The perpendicular component "3" of polarization contains the ferroelectric and background components:

$$P_3\left(\mathbf{r}, E_3\right) = P\left(\mathbf{r}, E_3\right) + \varepsilon_0 \left(\varepsilon_b^i - 1\right) E_3^i.$$

The electric displacement vector equals $\mathbf{D}^i = \varepsilon_0 \varepsilon_b^i \mathbf{E}^i + \mathbf{P}$ inside the particle and $\mathbf{D}^e = \varepsilon_0 \varepsilon^e \mathbf{E}^e$ outside it, where ε^e is the relative dielectric permittivity of external carriers. Hereafter, the superscripts i and e denote the electric field or the potential inside and outside the particle, respectively.

The non-uniform spatial distribution of the ferroelectric component of the polarization $P_3\left(\mathbf{r}, E_3\right)$ can be determined from the Landau–Ginzburg–Devonshire equation for the nanoparticle interior,

$$\alpha_{\mathrm{P}} P_3 + \beta_{\mathrm{P}} P_3^3 + \gamma_{\mathrm{P}} P_3^5 - \\ - g_{33mn} \frac{\partial^2 P_3}{\partial x_m \partial x_n} - 2 Q_{kli3} \sigma_{kl} P_3 = E_3, \qquad (5.1)$$

where the coefficient $\alpha_{\mathrm{P}}\left(T\right) = \alpha_{\mathrm{P}}^{(T)}\left(T - T_{\mathrm{C}}\right)$, T is the absolute temperature, T_{C} the Curie temperature of the paraelectric-ferroelectric phase transition, β_{P} and γ_{P} are the coefficients of the LGD potential expansion in a series in the polarization, and σ_{kl} and Q_{ijkl} are the tensors of elastic stresses and electrostriction, respectively. The flexoeffect is considered to be small. The boundary conditions for the polarization P_3 at the particle surface S are assumed to be standard, i.e. $\left(\partial P_3 / \partial \mathbf{n}\right)_S = 0$.

The electric field is determined, as usually, through the electric potential, $E_i = -\partial\varphi / \partial x_i$. For the combination ferroelectric-insulator, the electric potential φ can be found from the Laplace equation outside the nanoparticle, $\varepsilon_0 \varepsilon^e \Delta\varphi_e = 0$, and the Poisson equation inside it,

$$\varepsilon_0 \varepsilon_{ij}^b \frac{\partial^2 \phi}{\partial x_i \partial x_j} = \frac{\partial P_k}{\partial x_k}, \qquad (5.2)$$

where ε_{ij}^b is the background dielectric permittivity. There are no free charges inside the particle.

The continuity equation $\left(\varphi_e - \varphi_i\right)_S = 0$ is a required boundary condition for the electric potential at the particle surface. The boundary condition for the normal components of the electric displacement vector should involve the surface screening of the environment from free charges on the particle surface S: $\left[\left(\mathbf{D}_e - \mathbf{D}_i\right)\mathbf{n} + \varepsilon_0 \frac{\varphi_i}{\lambda}\right]_S = 0$, where λ is the screening length. The potential is constant at the particle-electrode interface: $\varphi_i|_{z=0} = 0$. The surface screening reduces the influence of an external field and diminishes the depolarization field associated with the polarization gradient.

In the framework of the phenomenological approach, the contribution of the linear and biquadratic ME couplings to the free energy of the system is described by the quantities $\mu_{ij} P_i M_j$ and $\xi_{ijkl} P_i P_j M_k M_l$, where $\mathbf{P}$ is the polarization and $\mathbf{M}$ the magnetization vector, μ_{ij} and ξ_{ijkl} are the tensors of corresponding ME effects [130–133]. The contribution of the PME effect is described by the term $\eta_{ijk}, P_i, M_j, M_k$ [127, 131]. To calculate the PME coefficients, the phenomenological LGD model is used [134, 135]. If the magnetization $\mathbf{M}$ is proportional to the applied magnetic field $\mathbf{H}$, i.e. $M \approx \chi_{\mathrm{FM}}\left(T\right) H$, the PME coefficient η has the form [128]

$$\eta\left(T\right) = -P_S\left(T\right) \chi_{\mathrm{FE}}\left(T\right) \left(\chi_{\mathrm{M}}\left(T\right)\right)^2 \xi_{\mathrm{MP}}, \qquad (5.3)$$

where $P_S\left(T\right)$ is the spontaneous polarization $P_3\left(\mathbf{r}\right)$ averaged over the volume, which is calculated from Eq. (5.1) at $H = 0$ and $E = 0$; and the functions $\chi_{\mathrm{M}}\left(T\right)$ and $\chi_{\mathrm{FE}}\left(T\right)$ are the linear magnetic susceptibility and the dielectric permittivity, respectively, of the ferroelectric phase averaged over the particle volume. The ferroelectric susceptibility can be calculated by formula (5.1) with the help of the equation

$$\chi_{\mathrm{FE}}\left(T\right) = \left.\frac{\partial \left\langle P_3 \right\rangle}{\partial E_3}\right|_{E_3 = 0}. \qquad (5.4)$$

The approximate expression for the magnetic susceptibility obtained in work [128] reads

$$\chi_{\mathrm{M}}\left(T\right) = \frac{\mu_0}{\alpha_{\mathrm{M}}^{(T)}\left(T - \theta\right) + \xi_{\mathrm{LM}} L^2 + \xi_{\mathrm{MP}} P_S^2\left(T\right)}. \qquad (5.5)$$

Equations (5.3) and (5.4) are valid for the ferroelectric-antiferromagnetic phase with a nonzero antiferromagnetic long-range order parameter (i.e. at $L \neq \neq 0$) and for the magnetically disordered ferroelectric-paramagnetic phase (i.e. at $M = L = 0$). The parameters ξ_{LM} and ξ_{MP} are biquadratic ME coefficients for

the polarization and magnetic order parameters in the ME energy

$$G_{\rm ME} = \frac{1}{2}\left(\xi_{\rm MP} M^2 + \xi_{\rm LP} L^2\right) P^2.$$

Note that only two coefficients in the magnetic energy

$$G_{\rm M} = \frac{\alpha_{\rm L}(T)}{2} L^2 + \frac{\beta_{\rm L}}{4} L^4 + \frac{\alpha_{\rm M}(T)}{2} M^2 + \\ + \frac{\beta_{\rm M}}{4} M^4 - \mu_0 M H + \frac{\xi_{\rm LM}}{2} L^2 M^2$$

are temperature-dependent; namely, these are

$$\alpha_{\rm L}(T) = \alpha_{\rm M}^{(T)}(T - T_{\rm N})$$

and

$$\alpha_{\rm M}(T) = \alpha_{\rm M}^{(T)}(T - \theta),$$

where $T_{\rm N}$ and θ are the Neél and Curie temperatures, respectively.

5.4. Analytical solutions

Using the finite-element method, the spatial distribution and the average electric field inside particles can be calculated. The material parameters of $BiFeO_3$ used in calculations [128] were as follows: the spontaneous polarization $P_S = 1$ m/C, the electrostriction coefficient $Q_{12} = -0.05$ m^4/C^2, the electrostriction coefficient $Q_{11} = -0.1$ m^4/C^2, the background dielectric constant $\varepsilon_b = 10$, the external dielectric constant $\varepsilon_e = 1$, the gradient coefficient $\gamma_{11} = 10^{-10}$ m^3/F, the LGD coefficient $\alpha_S = 10^{-4}$ m^2/F, the LGD coefficient $\beta = 10^7$ J m^5/C^4, the LGD coefficient $\alpha = -10^7$ m/F (at $T = 300$ K), the ferroelectric Curie temperature $T_{\rm C} = 1100$ K, the temperature coefficient $\alpha_T = 0.9 \times 10^6$ m/(C F), the Neél temperature $T_{\rm N} = 650$ K, the screening length $\lambda = 10^{-3} \div 10^2$ nm, and the dielectric constant $\varepsilon_0 = 8.85 \times 10^{-12}$ F/m.

The calculated numerical results were approximated analytically. The expression obtained for the electric field at the distance λ from the surface is as follows:

$$E_{dX} \approx -\frac{P_X}{\varepsilon_0} \frac{\lambda n_\infty(a,b,c)}{\lambda + R n_\infty(a,b,c)}, \tag{5.6}$$

where n_∞ is the depolarization factor of the system in bulk (the limit $\lambda \to \infty$) making no allowance for the charge screening, and R is a characteristic length along the particle semiaxis a. Using Eq. (5.6), the effective depolarization factor $n_d(a,b,c) = -\varepsilon_0 \frac{E_{dX}}{P_X}$ can be introduced, so that

$$n_d(a,b,c) = \frac{\lambda n_\infty(a,b,c)}{\lambda + R n_\infty(a,b,c)}. \tag{5.7}$$

Formula (5.7) allows the parameters n_∞ and R to be determined for a large variety of nanoparticle sizes a, b, and c, which are the lengths of ellipsoid semiaxes. The specific values of those parameters were found, by using the following approximations:

$$n_\infty(a,b,c) \approx \frac{b}{\varepsilon_b b + \varepsilon_e a}\left(\frac{c^2}{c^2 + 0.7a\,c + a^2 \frac{b}{b+0.075a}}\right), \tag{5.8a}$$

$$R(a,b,c) \approx a\left(0.62 + 0.19\frac{a}{b} + 0.25\frac{a}{c}\right). \tag{5.8b}$$

Note that the first multiplier in formula (5.8a) is an exact expression for the depolarization coefficient of the elliptic cylinder with the semiaxes a and b. A high accuracy of approximations (5.8) becomes evident from Figs. 5.2, *b*–*d*.

Taking Eqs. (5.6)–(5.8) into account, the transition temperature into the paraphase, $T_{\rm cr}(a,b,c)$, can be determined analytically from the condition $\alpha + \frac{n_d}{\varepsilon_0} = 0$ [128]; namely,

$$T_{\rm cr}(a,b,c) = T_{\rm C} - \frac{n_d(a,b,c)}{\alpha_T \varepsilon_0}. \tag{5.9}$$

This formula gives rise to analytical expressions for the average spontaneous polarization,

$$P_S = \begin{cases} \sqrt{\frac{\alpha_T}{\beta}\left(T_{\rm cr}(a,b,c) - T\right)} & \text{for } T < T_{\rm cr}, \\ 0 & \text{for } T > T_{\rm cr}, \end{cases} \tag{5.10}$$

$$\chi_{\rm FE}(T) = \begin{cases} \dfrac{1}{2\alpha_T\left(T_{\rm cr}(a,b,c) - T\right)} & \text{for } T < T_{\rm cr}, \\ \dfrac{1}{\alpha_T\left(T - T_{\rm cr}(a,b,c)\right)} & \text{for } T > T_{\rm cr}. \end{cases} \tag{5.11}$$

Furthermore, Eqs. (5.3), (5.5), (5.10), and (5.11) bring us to an analytical expression for the PME coefficient in the form

$$\eta(T) = \begin{cases} \dfrac{-\xi_{\rm MP}\left(\chi_{\rm M}(T)\right)^2}{2\sqrt{\alpha_T \beta\left(T_{\rm cr}(a,b,c) - T\right)}} & \text{for } T < T_{\rm cr}, \\ 0 & \text{for } T > T_{\rm cr}. \end{cases} \tag{5.12}$$

As follows from formulas (5.9)–(5.12), the depolarization fields considerably affect the polar and PME properties of ellipsoidal nanoparticles.

5.5. Influence of size effects on phase diagrams, average polarization, and PME coefficient

The phase diagrams of semiellipsoidal $BiFeO_3$ nanoparticles in the relative temperature T/T_C (T_C is the Curie temperature in bulk) – semiaxis length a coordinates are shown in Fig. 5.2, *a*. The boundary between the PE and FE phases, i.e. the actual phase transition temperature $T_{cr}(a, b, c)$, depends on the semiellipsoid sizes a, b, and c. The size effects manifest themselves in the disappearance of the ferroelectric phase at a critical size, which is followed by a monotonic growth of the transition temperature, as a increases, and its saturation at $a \gg 100$ nm. The curves in Fig. 5.2 were calculated for various length values of the semiaxis b = 3, 10, 30, and 100 nm and the fixed particle heights c = 10 nm (Fig. 5.2, *a*) and 100 nm (Fig. 5.2, *b*). The critical size monotonically decreases, and the PE-FE phase boundary shifts from left to right with the growth of b at a fixed c. The critical sizes calculated for c = 10 nm are considerably smaller than those calculated for c = 100 nm and the same b-values [cf. the curves in Figs. 5.2, *a* and 5.2, *b*]. At c = 10 nm, the critical size varies in a narrow interval of 10–12 nm, and the curves calculated for different b-values are located very close to one another. At c = 100 nm, the critical size changes in a wider interval of 15–45 nm, and the curves calculated for different b-values are well separated from one another.

The analysis of the calculation results depicted in Fig. 5.2 makes it possible to draw a conclusion that the influence of the size effect on the phase diagrams is considerable for the ratio bc/a^2 between the particle sizes and less sensitive to separate size magnitudes. The smaller this ratio, the lower is the depolarization field and, consequently, the higher is the transition temperature and the smaller is the critical size. This result seems to be non-trivial.

The dependences of the spontaneous polarization on the semiellipsoid length a calculated for room temperature and the semiaxis length c = 100 nm are shown in Fig. 5.2, *b*. The lengths of another semiaxis b are indicated near the curves. The polarization curves calculated for different b-values are well separated from one another. The spontaneous polarization appears at the critical size $a_{cr}(b, c)$ and increases

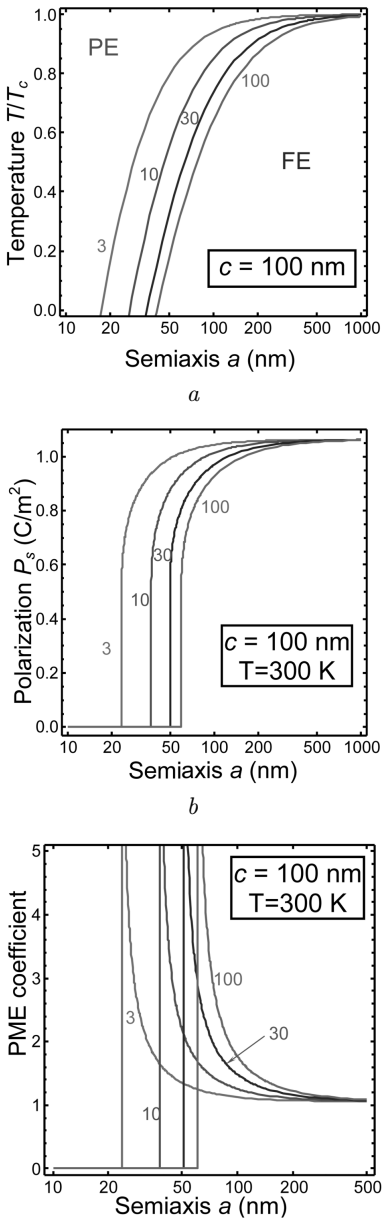

Fig. 5.2. Phase diagrams in the temperature T – ellipsoid semiaxis length a coordinates calculated for the semiaxis length c = 100 nm and various semiaxis lengths b = 3, 10, 30, and 100 nm (indicated near the curves) (*a*). Dependences of the spontaneous polarization on the ellipsoid semiaxis length a at room temperature calculated for c = 100 nm and various semiaxis lengths b = 3, 10, 30, and 100 nm (indicated near the curves) (*b*). The same as in panel *b*, but for the PME coefficient (*c*). The screening length λ = 1 nm, the other parameters corresponding to $BiFeO_3$ are quoted in section 5.2 (Adapted from [128], with the permission of AIP Publishing)

with a. The polarization saturates at a value of about 1 C/m^2 at $a \gg 100$ nm.

The dependences of the PME coefficient on the semiaxis length a calculated for room temperature and the semiaxis length $c = 100$ nm are shown in Fig. 5.2, *c*. The lengthsof another semiaxis b were chosen the same as in the previous figures ($b = 3$, 10, 30, and 100 nm). The plotted dependences were normalized by the main PME coefficient value. The PME coefficient equals zero, if $a < a_{\rm cr}\,(b, c)$ owing to the spontaneous disappearance of the polarization, appears at $a < a_{\rm cr}$, has a singularity at $a = a_{\rm cr}(b, c)$, then decreases, as the size a grows, and saturates at $a \gg 100$ nm. The singularity testifies to a possibility to obtain a giant PME effect in $BiFeO_3$ nanoparticles near the size-induced FE-PE phase transition point. In particular, the normalized PME coefficient significantly exceeds 1 for the sizes within the interval $a_{\rm cr}\,(b, c) \leq a < 2a_{\rm cr}\,(b, c)$. The behavior of the PME coefficient reproduces that of the dielectric susceptibility described by Eq. (5.11) in the framework of our model. The dependences of the PME coefficient calculated for various b-values are well separated from one another.

To summarize, in this section we considered the influence of nanoparticle sizes on the phase diagrams and the ferroelectric and magnetoelectric properties of semiellipsoidal $BiFeO_3$ nanoparticles attached to a rigid conductive substrate. In the framework of the Landau–Ginzburg–Devonshire method, as well as the classical electrostatics and elasticity theory, the spatial distributions of the spontaneous polarization vector inside the ferroelectric nanoparticles, the phase diagrams, and the PME coefficient were calculated. Analytical expressions were obtained for the dependences of the ferroelectric transition temperature, average polarization, linear dielectric susceptibility, and PME coefficient on the particle sizes in the general case of semiellipsoidal nanoparticles with different semiaxes a and b, and the height c. Since the depolarization field for nanoparticles with small c-values is substantially lower, the energy-beneficial are nanoparticle orientations along the spontaneous polarization plane $c < a$. As follows from the analysis of the results obtained, the phase diagrams, the spontaneous polarization, and the PME coefficient are quite sensitive to the ratio bc/a^2 between the particle sizes and are less sensitive to the size magnitudes. This circumstance opens a way to control the nanoparticle properties by choosing the proper value of this ratio.

6. Conclusions

Theoretical researches of the influence of the magnetoelectric effect on the physical properties of nanosized ferroics and multiferroics are very challenging. The interest in them has grown significantly within the last decade. The Landau–Ginzburg–Devonshire phenomenological theory can successfully describe the appearance of the piezomagnetic, piezoelectric, and linear magnetoelectric effects near the ferroic surface as a result of the surface-induced spontaneous reduction of a symmetry of the system. As a consequence, nanosized particles and thin ferroic films can manifest pronounced piezomagnetic, piezoelectric, and magnetoelectric properties, which are absent in the corresponding bulk materials. In particular, there may appear the giant magnetoelectric effect in nanowires induced by the surface tension. A significant influence of size effects and external fields on the magnetoelectric coupling coefficients, the dielectric, magnetic, and magnetoelectric susceptibilities in nanoferroics was considered. The special attention was paid to the influence of misfit deformations on the magnetoelectric coupling in thin ferroic films and the corresponding phase diagrams, including the emergence of new phases absent for the bulk material.

In the framework of the Landau–Ginzburg–Devonshire theory, the mechanisms giving rise to the appearance of the linear magnetoelectric and flexomagnetoelectric effects in nanoferroics induced by the flexomagnetic coupling are considered. A substantial influence of the flexomagnetoelectric effect on the susceptibility of nanoferroics is revealed. In particular, the sizes of semiellipsoidal bismuth ferrite nanoparticles strongly affect their polar and magnetoelectric properties.

1. M.D. Glinchuk, A.V. Ragulya, V.A. Stephanovich. *Nanoferroics* (Springer, 2013).
2. J. Tingting, C. Zhenxiang, Z. Hongyang, K. Hideo. Domain switching in single-phase multiferroics. *Appl. Phys. Rev.* **5**, 021102 (2018).
3. http://www.esrf.eu/UsersAndScience/Publications/Highlights/2009/elecstrmag.
4. P. Curie. Sur la symetrie dans les phénomènes physiques, symétrie d'un champ électrique et d'un champ magnétique. *J. Physique* **3**, 393 (1894).

5. L.D. Landau, E.M. Lifshitz. *Electrodynamics of Continuous Media* (Pergamon Press, 1984).
6. I.E. Dzyaloshinskii. To magnetoelectric effect in antiferromagnets. *Zh. Èksp. Teor. Fiz.* **37**, 881 (1959) (in Russian).
7. D.N. Astrov. The magnetoelectric effect in antiferromagnetics. *Sov. Phys. JETP* **11**, 708 (1960).
8. V.J. Folen, G.T. Rado, E.W. Stalder. Anisotropy of the magnetoelectric effect in Cr_2O_3. *Phys. Rev. Lett.* **6**, 607 (1961).
9. J. Zhai *et al.* Detection of pico-Tesla magnetic fields using magneto-electric sensors at room temperature. *Appl. Phys. Lett.* **88**, 062510 (2006).
10. A. Sundaresan, R. Bhargavi, N. Rangarajan, U. Siddesh, C.N.R. Rao. Ferromagnetism as a universal feature of nanoparticles of the otherwise nonmagnetic oxides. *Phys. Rev. B* **74**, 161306(R) (2006).
11. A.N. Morozovska, M.D. Glinchuk, E.A. Eliseev. Phase transitions induced by confinement of ferroic nanoparticles. *Phys. Rev. B* **76**, 014102 (2007).
12. E.A. Eliseev, M.D. Glinchuk, A.N. Morozovska. Appearance of ferroelectricity in thin films of incipient ferroelectric. *Phys. Status Solidi B* **244**, 3660 (2007).
13. M.D. Glinchuk, E.A. Eliseev, A.N. Morozovska, R. Blinc. Giant magnetoelectric effect induced by intrinsic surface stress in ferroic nanorods. *Phys. Rev. B* **77**, 024106 (2008).
14. M.D. Glinchuk A.N. Morozovska. The internal electric field originating from the mismatch effect and its influence on ferroelectric thin film properties. *J. Phys.: Condens. Matter.* **16**, 3517 (2004).
15. M.D. Glinchuk, A.N. Morozovska, E.A. Eliseev. Ferroelectric thin films phase diagrams with self-polarized phase and electret state. *J. Appl. Phys.* **99**, 114102 (2006).
16. J.F. Scott. Data storage: Multiferroic memories. *Nature Mater.* **6**, 256 (2007).
17. V.K. Wadhawan. *Introduction to Ferroic Materials* (Gordon and Breach, 2000).
18. E. Roduner. *Nanoscopic Materials. Size-Dependent Phenomena* (RSC Publishing, 2006).
19. B. Ruette, S. Zvyagin, A.P. Pyatakov, A. Bush, J.F. Li, V.I. Belotelov, A.K. Zvezdin, D. Viehland. Magnetic-field-induced phase transition in $BiFeO_3$ observed by high-field electron spin resonance: Cycloidal to homogeneous spin order. *Phys. Rev. B* **69**, 064114 (2004).
20. E.A. Eliseev, A.N. Morozovska, M.D. Glinchuk, B.Y. Zaulychny, V.V. Skorokhod, R. Blinc. Surface-induced piezomagnetic, piezoelectric, and linear magnetoelectric effects in nanosystems. *Phys. Rev. B* **82**, 085408 (2010).
21. E.A. Eliseev. Complete symmetry analyses of the surface-induced piezomagnetic, piezoelectric and linear magnetoelectric effects. *Ferroelectrics* **417**, 100 (2011).
22. M.D. Glinchuk, E.A. Eliseev, V.A. Stephanovich, R. Farhi. Ferroelectric thin film properties – Depolarization field and renormalization of a "bulk" free energy coefficients. *J. Appl. Phys.* **93**, 1150 (2003).
23. M.D. Glinchuk, A.N. Morozovska. Effect of surface tension and depolarization field on ferroelectric nanomaterial properties. *Phys. Status Solidi B* **238**, 81 (2003).
24. M.D. Glinchuk, I.V. Kondakova, V.V. Laguta, A.M. Slipenyuk, I.P. Bykov, A.V. Ragulya, V.P. Klimenko. Size effects in radiospectroscopy spectra of ferroelectric nanopowders. *Acta Physica Polonica A* **108**, 47 (2005).
25. J.S. Speck, W. Pompe. Domain configurations due to multiple misfit relaxation mechanisms in epitaxial ferroelectric thin films. I. Theory. *J. Appl. Phys.* **76**, 466 (1994).
26. L.D. Landau, E.M. Lifshitz. *Theory of Elasticity* (Butterworth-Heinemann, 1998).
27. V.I. Marchenko, A.Ya. Parshin. About elastic properties of the surface of crystals. *Zh. Èksp. Teor. Fiz.* **79**, 257 (1980) [*Sov. Phys. JETP* **52**, 129 (1980)].
28. V.A. Shchukin, D. Bimberg. Spontaneous ordering of nanostructures on crystal surfaces. *Rev. Mod. Phys.* **71**, 1125 (1999).
29. S. Dong, J.F. Li, D. Viehland. Giant magneto-electric effect in laminate composites. *Phil. Mag. Lett.* **83**, 769 (2003).
30. J. Wang, J.B. Neaton, H. Zheng, V. Nagarajan, S.B. Ogale, B. Liu, D. Viehland, V. Vaithyanathan, D.G. Schlom, U.V. Waghmare, N.A. Spaldin, K.M. Rabe, M. Wuttig, R. Ramesh. Epitaxial $BiFeO_3$ multiferroic thin film heterostructures. *Science* **299**, 1719 (2003).
31. W. Tian, V. Vaithyanathan, D.G. Schlom, Q. Zhan, S.Y. Yang, Y.H. Chu, R. Ramesh. Epitaxial integration of (0001) $BiFeO_3$ with (0001) GaN. *Appl. Phys. Lett.* **90**, 172908 (2007).
32. H. Naganuma, N. Shimura, J. Miura, H. Shima, Sh. Yasui, K. Nishida, T. Katoda, T. Iijima, H. Funakubo, S. Okamura. Enhancement of ferroelectric and magnetic properties in $BiFeO_3$ films by small amount of cobalt addition. *J. Appl. Phys.* **103**, 07E314 (2008).
33. M.D. Glinchuk, E.A. Eliseev, A.N. Morozovska, R. Blinc. Misfit strain induced magnetoelectric coupling in thin ferroic films. *J. Appl. Phys.* **105**, 084108 (2009).
34. V.V. Eremenko, V.A. Sirenko. *Magnetic and Magneto-Elastic Properties of Antiferromagnets and Superconductors* (Naukova Dumka, 2004) [in Russian].
35. A.N. Morozovska, M.D. Glinchuk, E.A. Eliseev, R. Blinc. Supplement in ArXiv. arxiv.org/abs/0803.4246v2.
36. M.I. Kaganov, V.M. Tsukernik. *Nature of Magnetism* (Nauka, 1982) [in Russian].
37. A.K. Tagantsev. Electric polarization in crystals and response to thermal and elastic perturbations. *Phase Trans.* **35**, 119 (1991).

38. W. Ma, L.E. Cross. Large flexoelectric polarization in ceramic lead magnesium niobate. *Appl. Phys. Lett.* **79**, 4420 (2001).
39. W. Ma, L.E. Cross. Flexoelectric polarization of barium strontium titanate in the paraelectric state. *Appl. Phys. Lett.* **81**, 3440 (2002).
40. W. Ma, L.E. Cross. Strain-gradient-induced electric polarization in lead zirconate titanate ceramic. *Appl. Phys. Lett.* **82**, 3293 (2003).
41. W. Ma, L.E. Cross. Flexoelectricity of barium titanate. *Appl. Phys. Lett.* **88**, 2902 (2006).
42. W. Ma. Flexoelectricity: Strain gradient effects in ferroelectrics. *Phys. Scr.* **129**, 180 (2007).
43. P. Zubko, G. Catalan, A. Buckley, P.R.L. Welche, J.F. Scott. Strain-gradient-induced polarization in $SrTiO_3$ single crystals. *Phys. Rev. Lett.* **99**, 167601 (2007).
44. G. Catalan, L.J. Sinnamon, J.M. Gregg. The effect of flexoelectricity on the dielectric properties of inhomogeneously strained ferroelectric thin films. *J. Phys.: Condens. Matter.* **16**, 2253 (2004).
45. G. Catalan, B. Noheda, J. McAneney, L.J. Sinnamond, J.M. Gregg. Strain gradients in epitaxial ferroelectrics. *Phys. Rev. B* **72**, 020102 (2005).
46. N.D. Sharma, C.M. Landis P.J. Sharma. Piezoelectric thin-film superlattices without using piezoelectric materials. *Appl. Phys.* **108**, 024304 (2010).
47. M. Gharbi, Z.H. Sun, P. Sharma, K. White, S. El-Borgi. Flexoelectric properties of ferroelectrics and the nanoindentation size-effect. *Int. J. Sol. Struct.* **48**, 249 (2011).
48. M.S. Majdoub, P. Sharma, T. Cagin. Enhanced size-dependent piezoelectricity and elasticity in nanostructures due to the flexoelectric effect. *Phys. Rev. B* **77**, 125424 (2008).
49. S.V. Kalinin, V. Meunier. Electronic flexoelectricity in low-dimensional systems. *Phys. Rev. B* **77**, 033403 (2008).
50. E.A. Eliseev, A.N. Morozovska, M.D. Glinchuk, R. Blinc. Spontaneous flexoelectric/flexomagnetic effect in nanoferroics. *Phys. Rev. B* **79**, 165433 (2009).
51. P. Lukashev, R.F. Sabirianov. Spin density in frustrated magnets under mechanical stress: Mn-based antiperovskites. *J. Appl. Phys.* **107** (9E), 115 (2010).
52. P. Lukashev, R.F. Sabirianov. Flexomagnetic effect in frustrated triangular magnetic structures. *Phys. Rev. B* **82**, 4417 (2010).
53. G. Rupprecht, R.O. Bell. Dielectric constant in paraelectric perovskites. *Phys. Rev.* **135**, 748 (1964).
54. *Modern Crystallography: Vol. IV. Physical Properties of Crystals.* Edited by L.A. Shuvalov (Springer, 1988).
55. D.B. Litvin. Magnetic physical-property tensors. *Acta Cryst. A* **50**, 406 (1994).
56. J.-P. Rivera. A short review of the magnetoelectric effect and related experimental techniques on single phase (multi-) ferroics. *Eur. Phys. J. B.* **71**, 299 (2009).
57. M.E. Lines, A.M. Glass. *Principles and Applications of Ferroelectrics and Related Phenomena* (Clarendon Press, 1977).
58. M.I. Kaganov, A.N. Omelyanchouk. Contribution to the phenomenological theory of a phase transition in a thin ferromagnetic plate. *Zh. Èksp. Teor. Fiz.* **34**, 895 (1972).
59. I. Rychetsky. Deformation of crystal surfaces in ferroelastic materials caused by antiphase domain boundaries. *J. Phys.: Condens. Matter.* **9**, 4583 (1997).
60. S.P. Alpay, I.B. Misirlioglu, A. Sharma, Z.-G. Ban. Structural characteristics of ferroelectric phase transformations in single-domain epitaxial films. *J. Appl. Phys.* **95**, 8118 (2004).
61. Z.-G. Ban, S.P. Alpay, J.V. Mantese. Fundamentals of graded ferroic materials and devices. *Phys. Rev. B* **67**, 4104 (2003).
62. G. Akcay, S.P. Alpay, G.A. Rossetti, J.F. Scott. Influence of mechanical boundary conditions on the electrocaloric properties of ferroelectric thin films. *J. Appl. Phys.* **103**, 4104 (2008).
63. Q.Y. Qiu, V. Nagarajan, S.P. Alpay. Film thickness versus misfit strain phase diagrams for epitaxial $PbTiO_3$ ultrathin ferroelectric films. *Phys. Rev. B* **78**, 064117 (2008).
64. E.A. Eliseev, M.D. Glinchuk, V. Khist, V.V. Skorokhod, R. Blinc, A.N. Morozovska. Linear magnetoelectric coupling and ferroelectricity induced by the flexomagnetic effect in ferroics. *Phys. Rev. B* **84**, 174112 (2011).
65. R. Perzynski, Y. Raikher. Surface effects in magnetic nanoparticles. In: *Effect of Surface Anisotropy on the Magnetic Resonance Properties of Nanosize Ferroparticles* (Springer, 2005), p. 141.
66. C.-L. Jia, V. Nagarajan, J.-Q. He, L. Houben, T. Zhao, R. Ramesh, K. Urban, R. Waser. Unit-cell scale mapping of ferroelectricity and tetragonality in epitaxial ultrathin ferroelectric films. *Nature Mater.* **6**, 64 (2007).
67. T. Moriya. Piezomagnetism in CoF_2. *J. Phys. Chem. Solids* **11**, 73 (1959).
68. G.A. Smolenskii, I.E. Chupis. Ferroelectromagnets. *Sov. Phys. Usp.* **25**, 475 (1982).
69. M. Fiebig. Revival of the magnetoelectric effect. *J. Phys. D* **38**, 123 (2005).
70. N.A. Spaldin, M. Fiebig. Materials science. The renaissance of magnetoelectric multiferroics. *Science* **309**, 391 (2005).
71. J.M. Rondinelli, N.A. Spaldin. Structure and properties of functional oxide thin films: Insights from electronic-structure calculations. *Adv. Mater.* **23**, 3363 (2011).
72. A.P. Pyatakov, A.K. Zvezdin. Magnetoelectric and multiferroic media. *Physics-Uspekhi* **55**, 557 (2012).
73. R. Ramesh, A.N. Spaldin. Multiferroics: progress and prospects in thin films. *Nature Mater.* **6**, 21 (2007).

74. P.J. Ryan, J.-W. Kim, T. Birol, P. Thompson, J.-H. Lee, X. Ke, P.S. Normile, E. Karapetrova, P. Schiffer, S.D. Brown, C.J. Fennie, D.G. Schlom. Reversible control of magnetic interactions by electric field in a single-phase material. *Nat. Commun.* **4**, 1334 (2013).
75. M.J. Haun, E. Furman, T.R. Halemane, L.E. Cross. Thermodynamic theory of the lead zirconate-titanate solid solution system. Part IV: Tilting of the oxygen octahedral. *Ferroelectrics* **99**, 55 (1989).
76. E.V. Balashova, A.K. Tagantsev. Polarization response of crystals with structural and ferroelectric instabilities. *Phys. Rev. B* **48**, 9979 (1993).
77. A.K. Tagantsev, E. Courtens, L. Arzel. Prediction of a low-temperature ferroelectric instability in antiphase domain boundaries of strontium titanate. *Phys. Rev. B* **64**, 224107 (2001).
78. S.L. Hou, N. Bloembergen. Paramagnetoelectric effects in $NiSO_4{\cdot}6\ H_2O$. *Phys. Rev.* **138**, 1218 (1965).
79. V.V. Shvartsman, S. Bedanta, P. Borisov, W. Kleemann. (Sr,Mn)TiO_3: A magnetoelectric multiglass. *Phys. Rev. Lett.* **101**, 165704 (2008).
80. B. Howes, M. Pelizzone, P. Fischer, C. Tabaresmunoz, J-P. Rivera, H. Schmid. Characterisation of some magnetic and magnetoelectric properties of ferroelectric $Pb(Fe_{1/2}Nb_{1/2})O_3$. *Ferroelectrics* **54**, 317 (1984).
81. T. Watanabe, K. Kohn. Magnetoelectric effect and low temperature transition of $PbFe_{0.5}Nb_{0.5}O_3$ single crystal. *Phase Trans.* **15**, 57 (1989).
82. W. Kleemann, V.V. Shvartsman, P. Borisov, A. Kania. Coexistence of antiferromagnetic and spin cluster glass order in the magnetoelectric relaxor multiferroic $PbFe_{0.5}Nb_{0.5}O_3$. *Phys. Rev. Lett.* **105**, 257202 (2010).
83. V.V. Laguta, A.N. Morozovska, E.A. Eliseev, I.P. Raevski, S.I. Raevskaya, E.I. Sitalo, S.A. Prosandeev L. Bellaiche. Room-temperature paramagnetoelectric effect in magnetoelectric multiferroics $Pb(Fe_{1/2}Nb_{1/2})O_3$ and its solid solution with $PbTiO_3$. *J. Mater. Sci.* **51**, 5330 (2016).
84. J. Seidel, L.W. Martin, Q. He, Q. Zhan, Y.-H. Chu, A. Rother, M.E. Hawkridge, P. Maksymovych, P. Yu, M. Gajek, N. Balke, S.V. Kalinin, S. Gemming, F. Wang, G. Catalan, J.F. Scott, N.A. Spaldin, J. Orenstein, R. Ramesh. Conduction at domain walls in oxide multiferroics. *Nature Mater.* **8**, 229 (2009).
85. J. Seidel, P. Maksymovych, Y. Batra, A. Katan, S.-Y. Yang, Q. He, A.P. Baddorf, S.V. Kalinin, C.-H. Yang, J.-C. Yang, Y.-H. Chu, E.K.H. Salje, H. Wormeester, M. Salmeron, R. Ramesh, W. Domain. Conductivity in La-doped $BiFeO_3$. *Phys. Rev. Lett.* **105**, 197603 (2010).
86. Q. He, C.-H. Yeh, J.-C. Yang, G. Singh-Bhalla, C.-W. Liang, P.-W. Chiu G., Catalan, L.W. Martin, Y.-H. Chu, J.F. Scott, R. Ramesh. Magnetotransport at domain walls in $BiFeO_3$, *Phys. Rev. Lett.* **108**, 067203 (2012).
87. G. Catalan, J. Seidel, R. Ramesh, J.F. Scott. Domain wall nanoelectronics. *Rev. Mod. Phys.* **84**, 119 (2012).
88. R.K. Vasudevan, A.N. Morozovska, E.A. Eliseev, J. Britson, J.-C. Yang, Y.-H. Chu, P. Maksymovych, L.Q. Chen, V. Nagarajan, S.V. Kalinin. Domain wall geometry controls conduction in ferroelectrics. *Nano Lett.* **12**, 5524 (2012).
89. A.N. Morozovska, K. Rama, P.M. Vasudevan, S.V. Kalinin, E.A. Eliseev. Anisotropic conductivity of uncharged domain walls in $BiFeO_3$. *Phys. Rev. B* **86**, 085315 (2012).
90. P. Fischer, M. Polomska, I. Sosnowska, M. Szymanski. Temperature dependence of the crystal and magnetic structures of $BiFeO_3$. *J. Phys. C* **13**, 1931 (1980).
91. G. Catalan, J.F. Scott. Physics and applications of bismuth ferrite. *Adv. Mater.* **21**, 1 (2009).
92. Y.-H. Chu, Z. Qian, L.W. Martin, M.P. Cruz, P.-L. Yang, G.W. Pabst, F. Zavaliche, S.-Y. Yang, J.-X. Zhang, L.-Q. Chen, D.G. Schlom, I.-N. Lin, T.-B. Wu, R. Ramamoorthy. Nanoscale domain control in multiferroic $BiFeO_3$ thin films. *Adv. Mater.* **18**, 2307 (2006).
93. Y.-H. Chu, L.W. Martin, M.B. Holcomb, M. Gajek, S.-J. Han, Q. He, N. Balke, C.-H. Yang, D. Lee, W. Hu, Q. Zhan, P.-L. Yang, A. Fraile-Rodríguez, A. Scholl, S.X. Wang, R. Ramesh. Electric-field control of local ferromagnetism using a magnetoelectric multiferroic. *Nature Mater.* **7**, 478 (2008).
94. P. Maksymovych, M. Huijben, M. Pan, S. Jesse, N. Balke, Y.-H. Chu, H.J. Chang, A.Y. Borisevich, A.P. Baddorf, G. Rijnders, D.H.A. Blank, R. Ramesh, S.V. Kalinin. Ultrathin limit and dead-layer effects in local polarization switching of $BiFeO_3$. *Phys. Rev. B* **85**, 014119 (2012).
95. C. Beekman, W. Siemons, M. Chi, N. Balke, J.Y. Howe, T.Z. Ward, P. Maksymovych, J.D. Budai, J.Z. Tischler, R. Xu, W. Liu, H.M. Christen. Ferroelectric self-poling, switching, and monoclinic domain configuration in $BiFeO_3$ thin films. *Adv. Funct. Mater.* **26**, 5166 (2016).
96. A.Y. Borisevich, O.S. Ovchinnikov, C.H. Jung, M.P. Oxley, Y. Pu, S. Jan, E.A. Eliseev, A.N. Morozovska, R. Ramesh, S.J. Pennycook, S.V. Kalinin. Beyond condensed matter physics on the nanoscale: The role of ionic and electrochemical phenomena in the physical functionalities of oxide materials. *ACS Nano* **4**, 6071 (2010).
97. N. Balke, B. Winchester, W. Ren, Y.H. Chu, A.N. Morozovska, E.A. Eliseev, M. Huijben, K.R. Vasudevan, P. Maksymovych, J. Britson, S. Jesse, I. Kornev, R. Ramesh, L. Bellaiche, L.Q. Chen, S.V. Kalinin. Enhanced electric conductivity at ferroelectric vortex cores in $BiFeO_3$. *Nature Phys.* **8**, 81 (2012).
98. Y.-M. Kim, A. Kumar, A. Hatt, A.N. Morozovska, A. Tselev, M.D. Biegalski, I. Ivanov, E.A. Eliseev, S.J. Pen-

nycook, J.M. Rondinelli, S.V. Kalinin, A.Y. Borisevich. Interplay of octahedral tilts and polar order in $BiFeO_3$ films. *Adv. Mater.* **25**, 2497 (2013).

99. R.K. Vasudevan, W. Wu, J.R. Guest, A.P. Baddorf, A.N. Morozovska, E.A. Eliseev, N. Balke, V. Nagarajan, P. Maksymovych. Domain wall conduction and polarization-mediated transport in ferroelectrics. Adv. *Funct. Mater.* **23**, 2592 (2013).
100. Y.-M. Kim, A. Morozovska, E. Eliseev, M. Oxley, R. Mishra, T. Grande, S. Selbach, S. Pantelides, S. Kalinin, A. Borisevich. Direct observation of ferroelectric field effect and vacancy-controlled screening at the $BiFeO_3/La_xSr_{1-x}MnO_3$ interface. *Nature Mater.* **13**, 1019 (2014).
101. B. Winchester, N. Balke, X.X. Cheng, A.N. Morozovska, S. Kalinin, L.Q. Chen. Electroelastic fields in artificially created vortex cores in epitaxial $BiFeO_3$ thin films. *Appl. Phys. Lett.* **107**, 052903 (2015).
102. J.F. Scott. Iso-structural phase transitions in $BiFeO_3$. *Adv. Mater.* **22**, 2106 (2010).
103. S. Layek, H.C. Verma. Magnetic and dielectric properties of multiferroic $BiFeO_3$ nanoparticles synthesized by a novel citrate combustion method. *Adv. Mat. Lett.* **3**, 533 (2012).
104. Fengzhen Huang, Zhijun Wang, Xiaomei Lu, Junting Zhang, Kangli Min, Weiwei Lin, Ruixia Ti, TingTing Xu, Ju He, Chen Yue, Jinsong Zhu. Peculiar magnetism of $BiFeO_3$ nanoparticles with size approaching the period of the spiral spin structure. *Sci. Rep.* **3**, 2907 (2013).
105. D. Yadlovker, S. Berger. Uniform orientation and size of ferroelectric domains. *Phys. Rev. B* **71**, 184112 (2005).
106. D. Yadlovker, S. Berger. Reversible electric field induced nonferroelectric to ferroelectric phase transition in single crystal nanorods of potassium nitrate. *Appl. Phys. Lett.* **91**, 173104 (2007).
107. D. Yadlovker, S. Berger. Nucleation and growth of single crystals with uniform crystallographic orientation inside alumina nanopores. *J. Appl. Phys.* **101**, 034304 (2007).
108. M.H. Frey, D.A. Payne. Grain-size effect on structure and phase transformations for barium titanate. *Phys. Rev. B* **54**, 3158 (1996).
109. Z. Zhao, V. Buscaglia, M. Viviani, M.T. Buscaglia, L. Mitoseriu, A. Testino, M. Nygren, M. Johnsson, P. Nanni. Grain-size effects on the ferroelectric behavior of dense nanocrystalline $BaTiO_3$ ceramics. *Phys. Rev. B* **70**, 024107 (2004).
110. E. Erdem, H.-Ch. Semmelhack, R. Bottcher, H. Rumpf, J. Banys, A. Matthes, H.-J. Glasel, D. Hirsch, E. Hartmann. Study of the tetragonal-to-cubic phase transition in $PbTiO_3$ nanopowders. *J. Phys.: Condens. Matter* **18**, 3861 (2006).
111. I.S. Golovina, S.P. Kolesnik, V. Bryksa, V.V. Strelchuk, I.B. Yanchuk, I.N. Geifman, S.A. Khainakov, S.V. Svechnikov, A.N. Morozovska. Defect driven ferroelectricity and magnetism in nanocrystalline $KTaO_3$. *Physica B.* **407**, 614 (2012).
112. I.S. Golovina, V.P. Bryksa, V.V. Strelchuk, I.N. Geifman, A.A. Andriiko. Size effects in the temperatures of phase transitions in $KNbO_3$ nanopowder. *J. Appl. Phys.* **113**, 144103 (2013).
113. I.S. Golovina, V.P. Bryksa, V.V. Strelchuk, I.N. Geifman. Phase transitions in the nanopowders $KTa_{0.5}Nb_{0.5}O_3$ studied by Raman spectroscopy. *Funct. Mater.* **20**, 75 (2013).
114. I.S. Golovina, V.P. Bryksa, V.V. Strelchuk, I.N. Geifman, A.A. Andriiko. Magnetic properties of nanocrystalline $KNbO_3$. *J. Appl. Phys.* **114**, 174106 (2013).
115. T. Yu, Z.X. Shen, W.S. Toh, J.M. Xue, J. Wang. Size effect on the ferroelectric phase transition in $SrBi_2Ta_2O_9$ nanoparticles. *J. Appl. Phys.* **94**, 618 (2003).
116. H. Ke, D.C. Jia, W. Wang, Y. Zhou. Ferroelectric phase transition investigated by thermal analysis and Raman scattering in $SrBi_2Ta_2O_9$ nanoparticles. *Solid State Phenom.* **121–123**, 843 (2007).
117. P. Perriat, J.C. Niepce, G. Caboche. Thermodynamic considerations of the grain size dependency of material properties: a new approach to explain the variation of the dielectric permittivity of $BaTiO_3$ with grain size. *J. Therm. Anal. Calorim.* **41**, 635 (1994).
118. H. Huang, C.Q. Sun, P. Hing. Surface bond contraction and its effect on the nanometric sized lead zirconate titanate. *J. Phys.: Condens. Matter* **12**, 127 (2000).
119. H. Huang, C.Q. Sun, Z. Tianshu, P. Hing. Grain-size effect on ferroelectric $Pb(Zr_{1?x}Ti_x)O_3$ solid solutions induced by surface bond contraction. *Phys. Rev. B* **63**, 184112 (2001).
120. M. Wenhui. Surface tension and Curie temperature in ferroelectric nanowires and nanodots. *Appl. Phys. A* **96**, 915 (2009).
121. A.N. Morozovska, E.A. Eliseev, M.D. Glinchuk. Ferroelectricity enhancement in confined nanorods: Direct variational method. *Phys. Rev. B* **73**, 214106 (2006).
122. A.N. Morozovska, I.S. Golovina, S.V. Lemishko, A.A. Andriiko, S.A. Khainakov, E.A. Eliseev. Effect of Vegard strains on the extrinsic size effects in ferroelectric nanoparticles. *Phys. Rev. B* **90**, 214103 (2014).
123. A.N. Morozovska, M.D. Glinchuk. Reentrant phase in nanoferroics induced by the flexoelectric and Vegard effects. *J. Appl. Phys.* **119**, 094109 (2016).
124. E.A. Eliseev, A.V. Semchenko, Y.M. Fomichov, M.D. Glinchuk, V.V. Sidsky, V.V. Kolos, Yu.M. Pleskachevsky, M.V. Silibin, N.V. Morozovsky, A.N. Morozovska. Surface and finite size effects impact on the phase diagrams, polar and dielectric properties of $(Sr,Bi)Ta_2O_9$

ferroelectric nanoparticles. *J. Appl. Phys.* **119**, 204104 (2016).

125. P. Perriat, J.C. Niepce, G. Caboche. Thermodynamic considerations of the grain size dependency of material properties: A new approach to explain the variation of the dielectric permittivity of $BaTiO_3$ with grain size. *J. Therm. Anal. Calorim.* **41**, 635 (1994).
126. H. Huang, C.Q. Sun, P. Hing. Surface bond contraction and its effect on the nanometric sized lead zirconate titanate. *J. Phys.: Condens. Matter* **12**, 127 (2000).
127. H. Huang, C.Q. Sun, Z. Tianshu, P. Hing. Grain-size effect on ferroelectric $Pb(Zr_{1-x}Ti_x)O_3$ solid solutions induced by surface bond contraction. *Phys. Rev. B* **63**, 184112 (2001).
128. V.V. Khist, E.A. Eliseev, M.D. Glinchuk, M.V. Silibin, D.V. Karpinsky, A.N. Morozovska. Size effects of ferroelectric and magnetoelectric properties of semi-ellipsoidal bismuth ferrite nanoparticles. *J. Alloys Comp.* **714**, 303 (2017).
129. A.K. Tagantsev, G. Gerra. Interface-induced phenomena in polarization response of ferroelectric thin films. *J. Appl. Phys.* **100**, 051607 (2006).
130. M. Fiebig. Revival of the magnetoelectric effect. *J. Phys. D* **38**, 123 (2005).
131. D. Rahmedov, S. Prosandeev, J. Íñiguez, L. Bellaiche. Magnetoelectric signature in the magnetic properties of antiferromagnetic multiferroics: Atomistic simulations and phenomenology. *Phys. Rev. B* **88**, 224405 (2013).
132. M.D. Glinchuk, E.A. Eliseev, Y. Gu, L.-G. Chen, V. Gopalan, A.N. Morozovska. Electric-field induced ferromagnetic phase in paraelectric antiferromagnets. *Phys. Rev. B* **89**, 101412 (2014).
133. M.D. Glinchuk, E.A. Eliseev, A.N. Morozovska. New room temperature multiferroics on the base of single-phase nanostructured perovskites. *J. Appl. Phys.* **116**, 054101 (2014).
134. V.V. Laguta, A.N. Morozovska, E.A. Eliseev, I.P. Raevski, S.I. Raevskaya, E.I. Sitalo, S.A. Prosandeev, L. Bellaiche. Room-temperature paramagnetoelectric effect in magnetoelectric multiferroics $Pb(Fe_{1/2}Nb_{1/2})O_3$ and its solid solution with $PbTiO_3$. *J. Mater. Sci.* **51**, 5330 (2016).
135. S. Prosandeev, I.A. Kornev, L. Bellaiche. Magnetoelectricity in $BiFeO_3$ films: First-principles based computations and phenomenology. *Phys. Rev. B* **83**, 020102 (2011).

Received 15.07.18.
Translated from Ukrainian by O.I. Voitenko

М.Д. Глинчук, В.В. Хіст

ВІДНОВЛЕННЯ ІНТЕРЕСУ ДО МАГНІТОЕЛЕКТРИЧНОГО ЕФЕКТУ У НАНОФЕРОЇКАХ

Р е з ю м е

Авторський огляд присвячено останнім теоретичним дослідженням впливу магнітоелектричного ефекту на фізичні властивості нанорозмірних фероїків і мультифероїків. Особливу увагу приділено застосуванню феноменологічної теорії Ландау–Гінзбурга–Девоншира для опису виникнення п'єзомагнітного, п'єзоелектричного і лінійного магнітоелектричного ефектів поблизу поверхні фероїків, як таких, що викликані спонтанним пониженням симетрії, індукованим поверхнею. Як наслідок, нанорозмірні частинки і тонкі плівки можуть проявляти виражені п'єзомагнітні, п'єзоелектричні і магнітоелектричні властивості, відсутні у відповідних об'ємних матеріалів, з яких вони зроблені. Зокрема можливе виникнення гігантського магнітоелектричного ефекту у нанодротах, індукованого поверхневим натягом. Розглянуто та відзначено значний вплив розмірних ефектів та зовнішніх полів на коефіцієнти магнітоелектричного зв'язку, діелектричну, магнітну та магнітоелектричну сприйнятливість у нанофероїках. Особлива увага приділена розгляду впливу деформацій невідповідності на магнітоелектричний зв'язок у тонких плівках фероїків, їх фазові діаграми, включаючи виникнення нових фаз, відсутніх в об'ємному матеріалі. В рамках теорії Ландау–Гінзбурга–Девоншира розглянуто виникнення лінійного магнітоелектричного та флексомагнітоелектричного ефектів у нанофероїках, індукованого флексомагнітним зв'язком. Відзначено значний вплив флексомагнітоелектричного ефекту на сприйнятливість нанофероїків. Огляд завершується конкретним прикладом впливу розмірних ефектів на полярні та магнітоелектричні властивості напівеліпсоїдальних наночастинок феріту вісмута.